eScholarship@UMassChan

PD-LI promotes rear retraction during persistent cell migration by altering integrin ß4 dynamics

Item Type	Journal Article
Authors	Wang, Mengdie;Xiong, Choua;Mercurio, Arthur M.
Citation	Wang M, Xiong C, Mercurio AM. PD-LI promotes rear retraction during persistent cell migration by altering integrin ß4 dynamics. J Cell Biol. 2022 May 2;221(5):e202108083. doi: 10.1083/jcb.202108083. Epub 2022 Mar 28. PMID: 35344032; PMCID: PMC8965106.
DOI	[10.1083/jcb.202108083](10.1083/jcb.202108083)
Journal	The Journal of cell biology
Rights	© 2022 Wang et al. This article is distributed under the terms of an Attribution–Noncommercial–Share Alike–No Mirror Sites license for the first six months after the publication date (see http://www.rupress.org/terms/). After six months it is available under a Creative Commons License (Attribution–Noncommercial–Share Alike 4.0 International license, as described at https://creativecommons.org/licenses/by-nc-sa/4.0/).;Attribution-NonCommercial-ShareAlike 4.0 International
Download date	2025-01-17 23:45:58
Item License	http://creativecommons.org/licenses/by-nc-sa/4.0/
Link to Item	https://hdl.handle.net/20.500.14038/52393

ARTICLE

PD-LI promotes rear retraction during persistent cell migration by altering integrin β4 dynamics

Mengdie Wang[1] , Choua Xiong[1] , and Arthur M. Mercurio[1]

Although the immune checkpoint function of PD-L1 has dominated its study, we report that PD-L1 has an unanticipated intrinsic function in promoting the dynamics of persistent cell migration. PD-L1 concentrates at the rear of migrating carcinoma cells where it facilitates retraction, resulting in the formation of PD-L1–containing retraction fibers and migrasomes. PD-L1 promotes retraction by interacting with and localizing the β4 integrin to the rear enabling this integrin to stimulate contractility. This mechanism involves the ability of PD-L1 to maintain cell polarity and lower membrane tension at the cell rear compared with the leading edge that promotes the localized interaction of PD-L1 and the β4 integrin. This interaction enables the β4 integrin to engage the actin cytoskeleton and promote RhoA-mediated contractility. The implications of these findings with respect to cell-autonomous functions of PD-L1 and cancer biology are significant.

Introduction

Directionally persistent cell migration underlies many biological processes, including embryogenesis, immune surveillance, wound healing, and tumor invasion (Petrie et al., 2009). It arises from intrinsic cell directionality or external signals that direct cells to establish polarity with defined leading and trailing edges with contraction and detachment at distinct regions of the cell to orchestrate cell motility (Petrie et al., 2009; Ridley et al., 2003). Although the mechanisms that drive protrusion at the cell front have been well characterized (Petrie et al., 2009; Ridley et al., 2003), less is known regarding the mechanisms regulating contractility and retraction at the rear of migrating cells. Considerable evidence implicates non-muscle myosin II and Rho GTPase signaling in the generation of the force needed for contractility (Ridley et al., 2003). More recent data have demonstrated the importance of membrane tension in rear retraction by a mechanism that involves the ability of caveolae to form in response to low membrane tension at the rear and orchestrate a RhoA signaling pathway that controls F-actin organization and contractility (Hetmanski et al., 2019). Despite these seminal advances, much needs to be learned about the cell surface receptors that contribute to the dynamics at the rear of cells during directionally persistent cell migration.

This study was inspired by reports that programmed death ligand 1 (PD-L1) can contribute to the migration of cancer cells, although no mechanisms have been proposed to explain this contribution (Yu et al., 2020b). PD-L1 is best known for its role in immune suppression in which it interacts with its receptor,

programmed cell death receptor 1 (PD-1), on T cells, resulting in T cell dysfunction (Zou et al., 2016). In contrast, relatively few studies have investigated tumor cell-intrinsic functions of PD-L1 that are independent of immune suppression, although recent work has revealed that it can also localize in the nucleus and contribute to such diverse processes as sister chromatid cohesion (Yu et al., 2020a) and pyroptosis (Hou et al., 2020). Here, we report that PD-L1 facilitates directionally persistent cell migration by promoting contractility at the cell rear by regulating the localization, cytoskeletal association, and signaling properties of the β4 integrin.

Results

PD-L1 facilitates directionally persistent cell migration independently of PD-1

Initially, we sought to determine how PD-L1 contributes to cell migration. We first assessed endogenous PD-L1 protein expression in different human cell lines, including MCF-10A (immortalized breast epithelial cells), MDA-MB-231 (breast carcinoma cells), and PC3 (prostate carcinoma cells; Fig. S1 A). Among these three cell lines, MDA-MB-231 cells expressed the highest cell-surface PD-L1 while PC3 cells expressed the lowest (Fig. S1 A). Despite these differences, depletion of PD-L1 expression using CRISPR/Cas9 in MDA-MB-231 cells and PC3 cells (Fig. 1, A and B; and Fig. S1 B) resulted in a marked inhibition of chemotaxis and invasion (Fig. 1, C and D). To assess whether this effect is
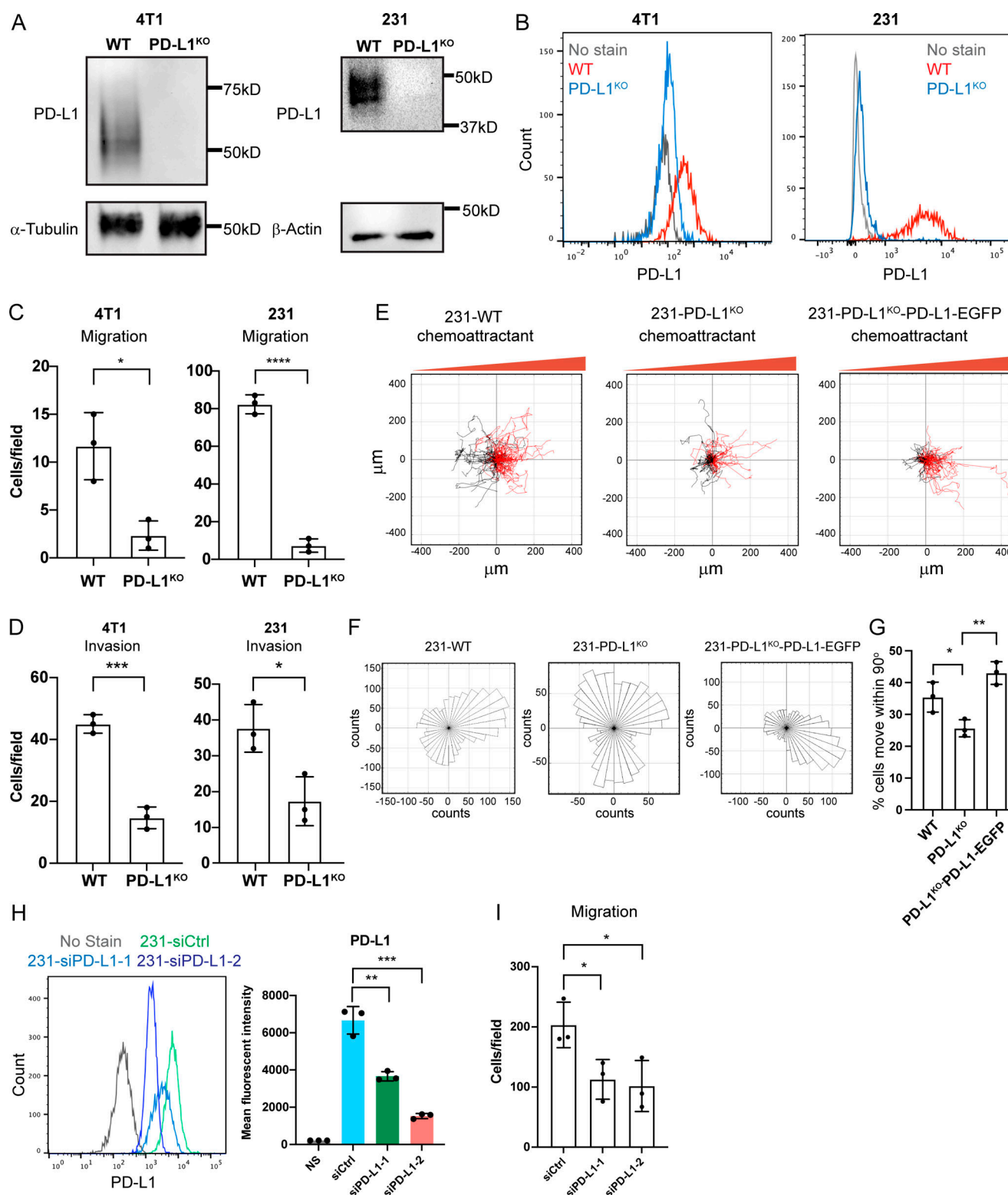
Figure 1. **PD-L1 regulates directional persistent cell migration and invasion. (A)** PD-L1 expression was depleted in MDA-MB-231 and 4T1 cells using CRISPR/Cas9, and protein levels were compared with WT cells by immunoblotting. The same α-tubulin immunoblot is shown in Fig. S3 B. **(B)** Flow cytometry of cell surface PD-L1 in WT and PD-L1^KO MDA-MB-231 and 4T1 cells. **(C)** Trans-well migration assays comparing cell migration in WT and PD-L1^KO MDA-MB-231 and 4T1 cells. Data are shown as means ± SD from three independent experiments. Statistical significance was determined by two-sided, unpaired t test. *, 0.05 > P ≥ 0.01; ****, 0.0001 > P. **(D)** Trans-well invasion assays comparing cell migration in WT and PD-L1^KO MDA-MB-231 and 4T1 cells. Data are shown as means ± SD from three independent experiments. Statistical significance was determined by two-sided, unpaired t test. *, 0.05 > P ≥ 0.01; ***, 0.001 > P ≥ 0.0001. **(E)** Representative trajectories quantified based on the chemotaxis assay from three independent experiments: WT: n = 104 cells, PD-L1^KO: n = 93 cells, and PD-L1^KO-PD-L1-EGFP: n = 86 cells. **(F)** Rose plot diagrams show the direction of cell migration from the chemotaxis assay from three independent

experiments: WT: n = 104 cells, PD-L1^{KO}: n = 93 cells, and PD-L1^{KO}-PD-L1-EGFP: n = 86 cells. **(G)** Quantification of the directionality of cells from the chemotaxis assay. Data are shown as means ± SD from three independent experiments. Statistical significance was determined by two-sided, unpaired t test. *, 0.05 > P ≥ 0.01; **, 0.01 > P ≥ 0.001. **(H)** Flow cytometry and quantification of cell surface PD-L1 in siCtrl and siPD-L1 MDA-MB-231. Data are shown as means ± SD from three independent experiments. Statistical significance was determined by two-sided, unpaired t test. **, 0.01 > P ≥ 0.001; ***, 0.001 > P ≥ 0.0001. **(I)** Trans-well migration assays comparing cell migration in siCtrl and siPD-L1 MDA-MB-231 cells. Data are shown as means ± SD from three independent experiments. Statistical significance was determined by two-sided, unpaired t test. *, 0.05 > P ≥ 0.01. Source data are available for this figure: SourceData F1.

conserved across species, we depleted endogenous PD-L1 in 4T1 murine breast carcinoma cells (Fig. 1, A and B) and observed similar results (Fig. 1, C and D). To investigate this migration in more detail, we expressed PD-L1 tagged with enhanced GFP (PD-L1-EGFP) using a lentiviral system in PD-L1 knockout MDA-MB-231 and PC3 cells (Fig. S1 C), which rescued chemotaxis (Fig. S1 D). Further, time-lapse microscopy confirmed that loss of PD-L1 impaired migration and that migration was restored upon expression of PD-L1-EGFP (Fig. S1 E). More rigorous data were obtained by tracking the migration of individual cells toward a gradient of chemoattractant (lysophosphatidic acid [LPA]) using time-lapse microscopy (Fig. 1 E), a state-of-the-art technique to study persistent cell migration (Kamakura et al., 2013; Laganenka et al., 2016; Zengel et al., 2011). Analysis of these videos revealed that PD-L1 WT cells exhibited persistent migration toward the chemoattractant (Fig. 1, E–G). Depletion of PD-L1 expression, however, resulted in a switch from persistent to random cell migration and re-expression of PD-L1 restored persistent migration (Fig. 1, E–G). Depletion of PD-L1 in MDA-MB-231 cells using siRNA also resulted in significant loss of chemotaxis (Fig. 1, H and I). The ability of PD-L1 to promote persistent cell migration appears to be independent of its interaction with PD-1 because the cell lines we investigated express undetectable levels of PD-1 (Fig. S1 F). Together, these data reveal a novel function for PD-L1 in facilitating persistent cell migration that is independent of PD-1.

PD-L1 concentrates at the cell rear and promotes rear retraction generating PD-L1 containing retraction fibers and migrasomes

We next sought to investigate the contribution of PD-L1 to persistent cell migration in more detail. Although PD-L1 is expressed on the cell surface, its spatial distribution has not been investigated especially during the dynamic process of cell migration. We used high-resolution time-lapse microscopy to track PD-L1 localization during migration in MDA-MB-231 cells that express PD-L1-EGFP upon deletion of endogenous PD-L1 (Fig. S1 C). Strikingly, PD-L1 was observed to concentrate at the rear of the cell in a distinct structure that moved in the direction of rear retraction, leaving behind retraction fibers that contained PD-L1 (Fig. 2 A and Video 1). Interestingly, we also observed that PD-L1 localizes in vesicular structures at the tips and intersections of retraction fibers that appear to be migrasomes (Fig. 2 A and Video 1). Migrasomes are a vesicular organelle that form from retraction fibers in migrating cells and can release exosome-like vesicles, as well as their cytoplasmic content, during cell migration (da Rocha-Azevedo and Schmid, 2015; Ma et al., 2015). This unexpected pattern of PD-L1 localization in distinct structures at the cell rear that coincided with rear retraction and

subsequently in retraction fibers and vesicular structures was also observed in 4T1 and PC3 cells that express PD-L1-EGFP (Fig. 2, B and C; and Video 2). We validated our observation that PD-L1 is localized in retraction fiber and migrasomes using multiplex immunofluorescent microscopy to demonstrate that endogenous PD-L1 co-localizes with F-actin and exhibits a punctate distribution in structures that resemble retraction fibers (Fig. 2 D). We also used fluorescently tagged wheat-germ agglutinin (WGA) as a marker for migrasomes (Chen et al., 2019), and observed that PD-L1 indeed co-localizes with WGA (Fig. 2 E). These data demonstrate that PD-L1 is localized in retraction fibers and migrasomes that form from rear retraction.

To determine if PD-L1 is required for rear cell dynamics during cell migration, we used SiR-actin for time-lapse microscopy to track F-actin in migrating WT and PD-L1 knockout MDA-MB-231 cells (Fig. 2 F; and Videos 3 and 4). WT cells adopted a mesenchymal-type, elongated mode of movement with F-actin organized in a front–rear polarity axis (Fig. 2 F; and Videos 3 and 4). In contrast, PD-L1 knockout cells were unable to establish clear front–rear polarity, and they formed random membrane protrusions (Fig. 2 F and Video 4). Quantifying these videos revealed that PD-L1 knock-out resulted in significantly shorter retraction fibers in both MDA-MB-231 and 4T1 cells (Fig. 2 G), which is probably a consequence of their loss of rear retraction.

To determine if PD-L1 promotes migrasome formation independently of cell migration, we quantified migrasome number/per length of retraction fibers using WGA as the migrasome marker based on the assumption that retraction fiber length correlates with migration. PD-L1 knockout cells had significantly fewer migrasomes/per length of retraction fibers than WT cells, and re-expression of PD-L1 in PD-L1 knockout cells rescued migrasome formation (Fig. 2, H and I). These data reveal that PD-L1 promotes rear retraction resulting in the generation of PD-L1 containing retraction fibers and migrasomes.

PD-L1 localizes the β4 integrin to the cell rear, enabling it to facilitate rear retraction and persistent migration

We next investigated the mechanism of how PD-L1 regulates rear retraction focusing on the potential role of integrins because of their importance in cell migration and migrasome formation (Ma et al., 2015; Wu et al., 2017). Initially, we assessed the contribution of different ECM proteins to the formation of retraction fibers. MDA-MB-231 cells were plated on coverslips coated with either laminin-332 or collagen-I and analyzed. Cells plated on laminin-332 coated coverslips formed PD-L1 containing retraction fibers and migrasomes (Fig. 3 A). However, cells plated on collagen-I exhibited a diffuse membrane localization of PD-L1 (Fig. 3 B) and formed significantly shorter retraction fibers
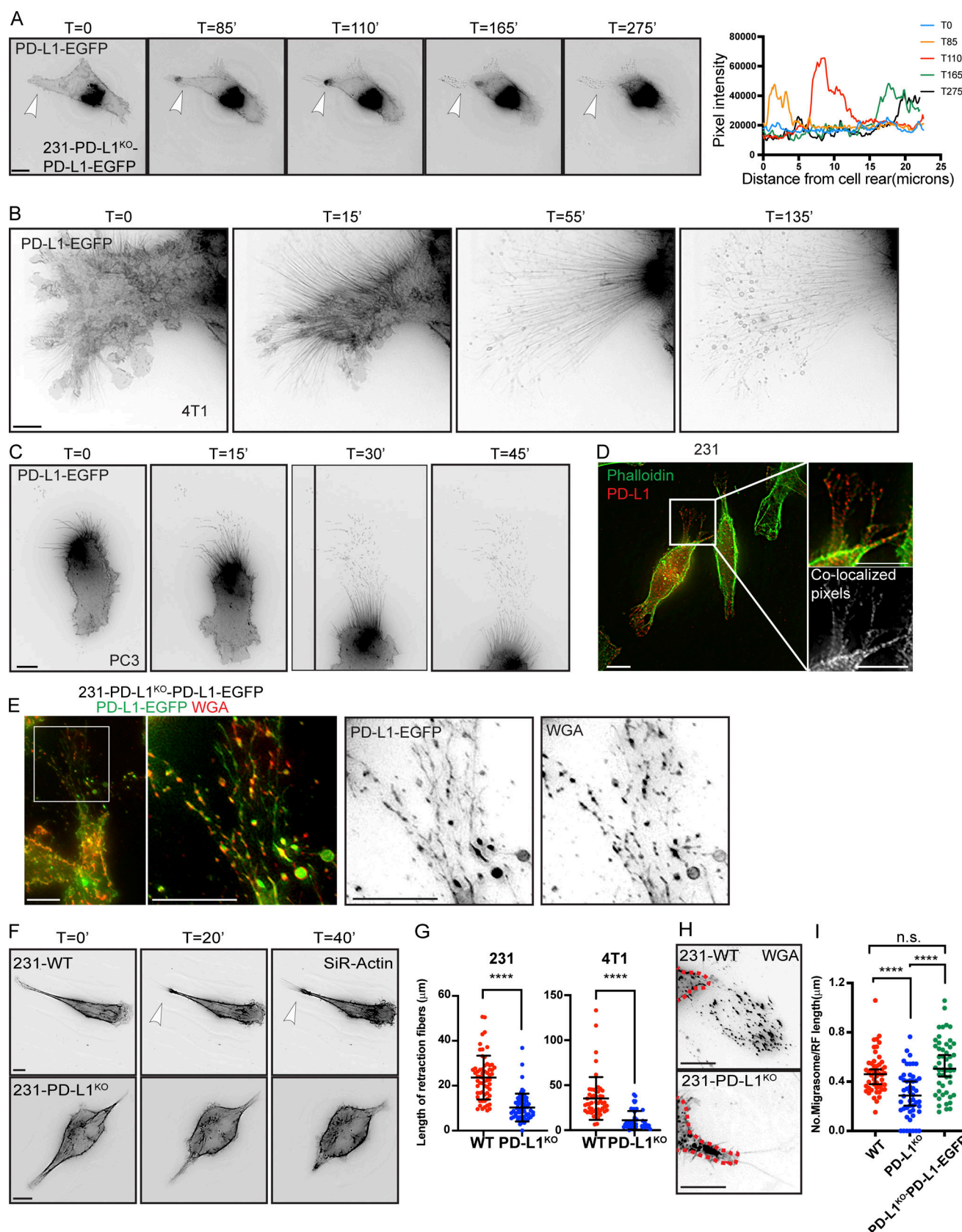
Figure 2. **PD-L1 concentrates at the cell rear and promotes rear retraction generating PD-L1 containing retraction fibers and migrasomes. (A)** Left: Representative time-lapse microscopy images of PD-L1^KO-PD-L1-EGFP MDA-MB-231 cells show PD-L1 expression during the formation of retraction fibers and migrasomes. Scale bar: 10 μm. Right: Quantification of PD-L1 signal from the rear toward inner cell body over time. Arrowheads indicate retracting cell rear.

(B) Representative time-lapse microscopy images of 4T1-PD-L1-EGFP cells show PD-L1 localizes at retraction fibers and migrasomes. Scale bar: 10 µm. **(C)** Representative time-lapse microscopy images of PD-L1-EGFP PC3 cells show PD-L1 localizes at retraction fibers and migrasomes. Scale bar: 10 µm. **(D)** A representative image of WT MDA-MB-231 cells stained with F-actin (phalloidin, green) and PD-L1 (red). Co-localization pixels of PD-L1 and F-actin are shown in the black-white image on the bottom right. Scale bar: 10 µm. **(E)** Images of PD-L1-EGFP (green) and WGA (red) in migrating cells. The boxed region outlines retraction fibers and migrasomes. Single-channel images are shown as black-white image. Scale bar: 10 µm. **(F)** Representative time-lapse microscopy images of WT (top) or PD-L1[KO] (bottom) MDA-MB-231 cells pre-labeled with SiR-Actin. Scale bar: 10 µm. Arrowheads point to cell rear and retraction fibers. **(G)** Quantification of retraction fiber length from images of WT or PD-L1[KO] MDA-MB-231 and 4T1 cells. Data are shown as means ± SD from three independent experiments, $n > 50$ cells per condition. Statistical significance was determined by two-sided, unpaired t test. ****, $0.0001 > P$. **(H)** Images of WGA labeled retraction fibers and migrasomes in 231-WT (upper) and 231-PD-L1[KO] cells (bottom). Scale bars: 10 µm. Red dotted lines outline cell body. **(I)** Quantification of migrasome numbers/retraction fiber length. Data are shown as means ± SD from three independent experiments, $n > 50$ cells per condition. Statistical significance was determined by two-sided, unpaired t test. ****, $0.0001 > P$.

compared with cells plated on laminin-332 (Fig. 3 C). Given that laminin-332 is a ligand for the α6β4 integrin (β4), this observation is consistent with previous reports that this integrin localizes at retraction fibers in migrating carcinoma cells (Rabinovitz and Mercurio, 1997; Wang et al., 2019; Fig. 3 D) and that PD-L1 and the β4 integrin can co-immunoprecipitate (Wang et al., 2018). However, the spatial interaction between PD-L1 and β4 has not been assessed in situ. For this reason, we performed a proximity ligation assay (PLA) that detects protein–protein associations within a 40 nm range (Alam, 2018) and observed that PD-L1 and β4 integrin interact in puncta located at the tips and intersections of retraction fibers, as well as in intracellular vesicles (Fig. 3, E and F). We also performed a PLA assay to assess the interaction between PD-L1 and β1 integrin subunit as a comparison using the α3 integrin as a positive control for β1 integrin interaction (Fig. 3, E and F). The number of foci per cell between PD-L1 and the β4 integrin was significantly more than the foci per cell between PD-L1 and the β1 integrin (Fig. 3, E and F). Thus, our data indicate that PD-L1 preferentially associates with the β4 integrin.

To analyze the dynamics of PD-L1 and the β4 integrin during cell migration, we tagged endogenous β4 with the fluorescent protein tdTomato in 4T1 cells using a CRISPR/Cas9 system that we previously established (Elaimy et al., 2019; designated as 4T1-β4-tdTomato) and then expressed PD-L1-EGFP in these cells (Fig. S2 A). We then performed time-lapse microscopy to track integrin β4-tdTomato and PD-L1-EGFP in migrating cells. Our data show that β4 integrin co-localizes with PD-L1 at the cell rear and later that these two molecules co-localize in retraction fibers and migrasomes that form while the rear retracts (Fig. 3 G and Video 5). We also observed that PD-L1 and the β4 integrin co-localize at F-actin–containing protrusions in fixed MDA-MB-231 cells (Fig. S2, B, and C). In live cells expressing PD-L1-EGFP, the β4 integrin co-localizes with PD-L1 in puncta in retraction fibers that have been hypothesized to specify the site of migrasome formation (Ma et al., 2015; Wu et al., 2017; Fig. 3 H). An important issue based on our findings is whether the contribution of integrin β4 to rear retraction is dependent on its interaction with laminin-332. Carcinoma cells, such as MDA-MB-231 cells, express laminin-332 (Fig. S2 D), which has a key role in migration (Mercurio et al., 2001). When WT cells were cultured on coverslips that were coated with different amounts of laminin-332, the length of retraction fibers and migrasome number/per length of retraction fibers significantly increased with increasing concentration of laminin-332 (Fig. 3, I and J). Interestingly, we
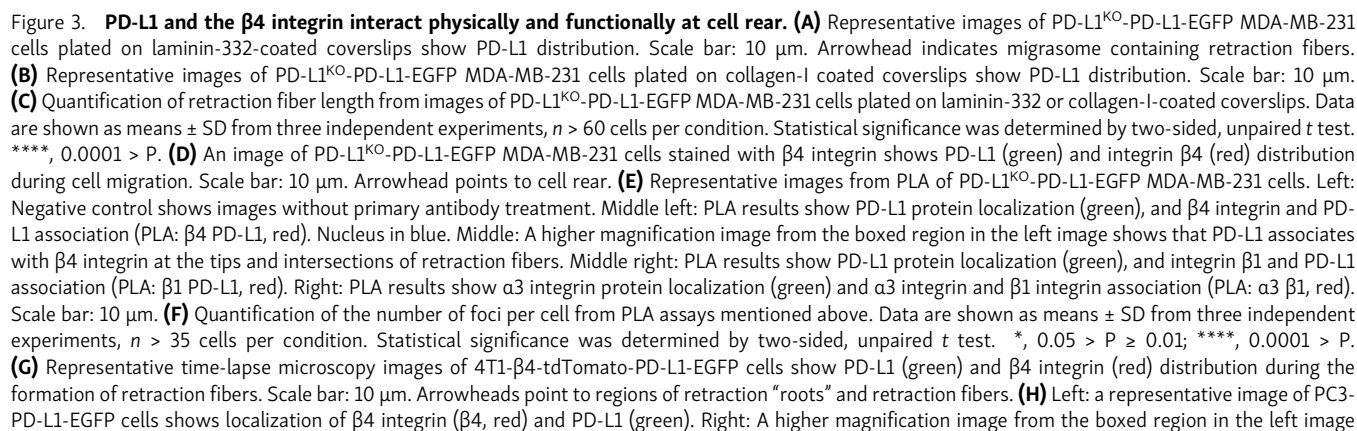
observed the same results in PD-L1 knockout cells, suggesting that the activation of β4 signaling upon engaging with laminin-332 is downstream of PD-L1 in mediating cell rear retraction.

We observed that PD-L1 regulates β4 integrin localization to the rear without affecting its expression (Fig. S3, A and B). In marked contrast, loss of PD-L1 resulted in a diffusion of β4 on the cell surface but it did not affect its localization in intracellular vesicles (Fig. 4, A and B), indicating that one function of PD-L1 is to localize β4 to the rear of migrating cells at sites of cell retraction.

To assess the contribution of the β4 integrin to rear retraction, we generated a doxycycline (dox)-inducible integrin β4 knockdown in 4T1-β4-tdTomato cells (designated as 4T1-dox-shβ4; Fig. S3 C). About 80% of these cells lose surface expression of the β4 integrin after treatment with dox for 3 days (Fig. S3, D–F). In the absence of dox, 4T1-dox-shβ4 cells formed F-actin–containing protrusions resembling retraction fibers and migrasomes that were enriched with PD-L1 and integrin β4 (Fig. 4 C), like MDA-MB-231 and PC3 cells (Fig. 3, D and H). However, upon dox treatment, these cells exhibited fewer actin-containing protrusions (Fig. 4 C). Subsequently, we expressed PD-L1-EGFP in 4T1-dox-shβ4 cells and used time-lapse microscopy to track PD-L1 localization during cell migration in the presence or absence of the β4 integrin. Without dox, cells exhibited persistent migration (Video 6). As the rear retracted, PD-L1 containing retraction fibers and migrasomes formed (Fig. 4 D and Video 6). In response to dox treatment, PD-L1 plasma membrane expression did not change (Fig. S3 G), but dox-treated cells were not able to commit to migration in one direction (Fig. 4 D and Video 7) like PD-L1 knockout cells. Also, shorter PD-L1 containing protrusions were present at multiple edges of the cells compared with the long retraction fibers at the rear in control cells (Fig. 4, D and E), suggesting defects in rear retraction in dox-treated cells. Similar results were obtained with MDA-MB-231 using siRNA to diminish β4 expression (Fig. S3 H) and SiR-actin to visualize migration dynamics (Fig. 4 F). In addition, knockdown of β4 integrin using siRNA significantly inhibited chemotaxis in these cells (Fig. S3 I), phenocopying loss of PD-L1. These data indicate that the β4 integrin promotes rear retraction during persistent cell migration.

PD-L1 is required to maintain front–rear polarity during migration

Given that cells without PD-L1 show loss of front–rear polarity morphologically (Fig. 2 F and Video 4), we investigated whether PD-L1 has a causal role in polarity. We used the PIP3 biosensor

Wang et al.
PD-LI regulates persistent migration

Journal of Cell Biology 5 of 19
https://doi.org/10.1083/jcb.202108083

Figure 3. **PD-L1 and the β4 integrin interact physically and functionally at cell rear. (A)** Representative images of PD-L1[KO]-PD-L1-EGFP MDA-MB-231 cells plated on laminin-332-coated coverslips show PD-L1 distribution. Scale bar: 10 μm. Arrowhead indicates migrasome containing retraction fibers. **(B)** Representative images of PD-L1[KO]-PD-L1-EGFP MDA-MB-231 cells plated on collagen-I coated coverslips show PD-L1 distribution. Scale bar: 10 μm. **(C)** Quantification of retraction fiber length from images of PD-L1[KO]-PD-L1-EGFP MDA-MB-231 cells plated on laminin-332 or collagen-I-coated coverslips. Data are shown as means ± SD from three independent experiments, $n > 60$ cells per condition. Statistical significance was determined by two-sided, unpaired t test. ****, $0.0001 > P$. **(D)** An image of PD-L1[KO]-PD-L1-EGFP MDA-MB-231 cells stained with β4 integrin shows PD-L1 (green) and integrin β4 (red) distribution during cell migration. Scale bar: 10 μm. Arrowhead points to cell rear. **(E)** Representative images from PLA of PD-L1[KO]-PD-L1-EGFP MDA-MB-231 cells. Left: Negative control shows images without primary antibody treatment. Middle left: PLA results show PD-L1 protein localization (green), and β4 integrin and PD-L1 association (PLA: β4 PD-L1, red). Nucleus in blue. Middle: A higher magnification image from the boxed region in the left image shows that PD-L1 associates with β4 integrin at the tips and intersections of retraction fibers. Middle right: PLA results show PD-L1 protein localization (green), and integrin β1 and PD-L1 association (PLA: β1 PD-L1, red). Right: PLA results show α3 integrin protein localization (green) and α3 integrin and β1 integrin association (PLA: α3 β1, red). Scale bar: 10 μm. **(F)** Quantification of the number of foci per cell from PLA assays mentioned above. Data are shown as means ± SD from three independent experiments, $n > 35$ cells per condition. Statistical significance was determined by two-sided, unpaired t test. *, $0.05 > P \geq 0.01$; ****, $0.0001 > P$. **(G)** Representative time-lapse microscopy images of 4T1-β4-tdTomato-PD-L1-EGFP cells show PD-L1 (green) and β4 integrin (red) distribution during the formation of retraction fibers. Scale bar: 10 μm. Arrowheads point to regions of retraction "roots" and retraction fibers. **(H)** Left: a representative image of PC3-PD-L1-EGFP cells shows localization of β4 integrin (β4, red) and PD-L1 (green). Right: A higher magnification image from the boxed region in the left image

show co-localization of β4 integrin (β4, red) and PD-L1 (green) in retraction fibers. Scale bar: 10 μm. **(I)** Quantification of length of retraction fibers in WT or PD-L1[KO] MDA-MB-231 cells when glass-bottomed dishes were coated with different concentrations of laminin-332 (LM332). Data are shown as means ± SD (n = 50 cells per condition, three independent experiments). Statistical significance was determined by two-sided, unpaired t test. *, $0.05 > P \geq 0.01$; **, $0.01 > P \geq 0.001$; ***, $0.001 > P \geq 0.0001$. **(J)** Quantification of numbers of migrasomes/length of retraction fibers in WT or PD-L1[KO] MDA-MB-231 cells when glass-bottomed dishes were coated with different concentrations of laminin-332 (LM332). Data are shown as means ± SD (n = 50 cells per condition, three independent experiments). Statistical significance was determined by two-sided, unpaired t test. **, $0.01 > P \geq 0.001$; **** $0.0001 > P$.

---

pleckstrin homology domain of the AKT protein kinase tagged with GFP (PH-AKT-GFP), which is recruited selectively to the membrane at the leading edge in response to a chemoattractant (Meili et al., 1999; Servant et al., 2000). PH-AKT-GFP was observed at the front of migrating cells in WT MDA-MB-231 cells (Fig. 5, A and B). However, PD-L1 knockout cells did not exhibit a polarized distribution of PH-AKT-GFP (Fig. 5, A and B) although they were able to recruit PH-AKT-GFP to the membrane,

indicating a loss of polarity. We also investigated the localization of ezrin, a member of the ezrin/radixin/moesinfamily that links the plasma membrane to the actin cortex upon phosphorylation (Bretscher et al., 2002) and is strongly enriched at the rear of migrating cells (Lorentzen et al., 2011; Olguin-Olguin et al., 2021). As expected, ezrin localized preferentially at cell rear in WT MDA-MB-231 cells (Fig. 5, C and D), and this polarized distribution was diminished in PD-L1 knockout cells (Fig. 5, C and D).
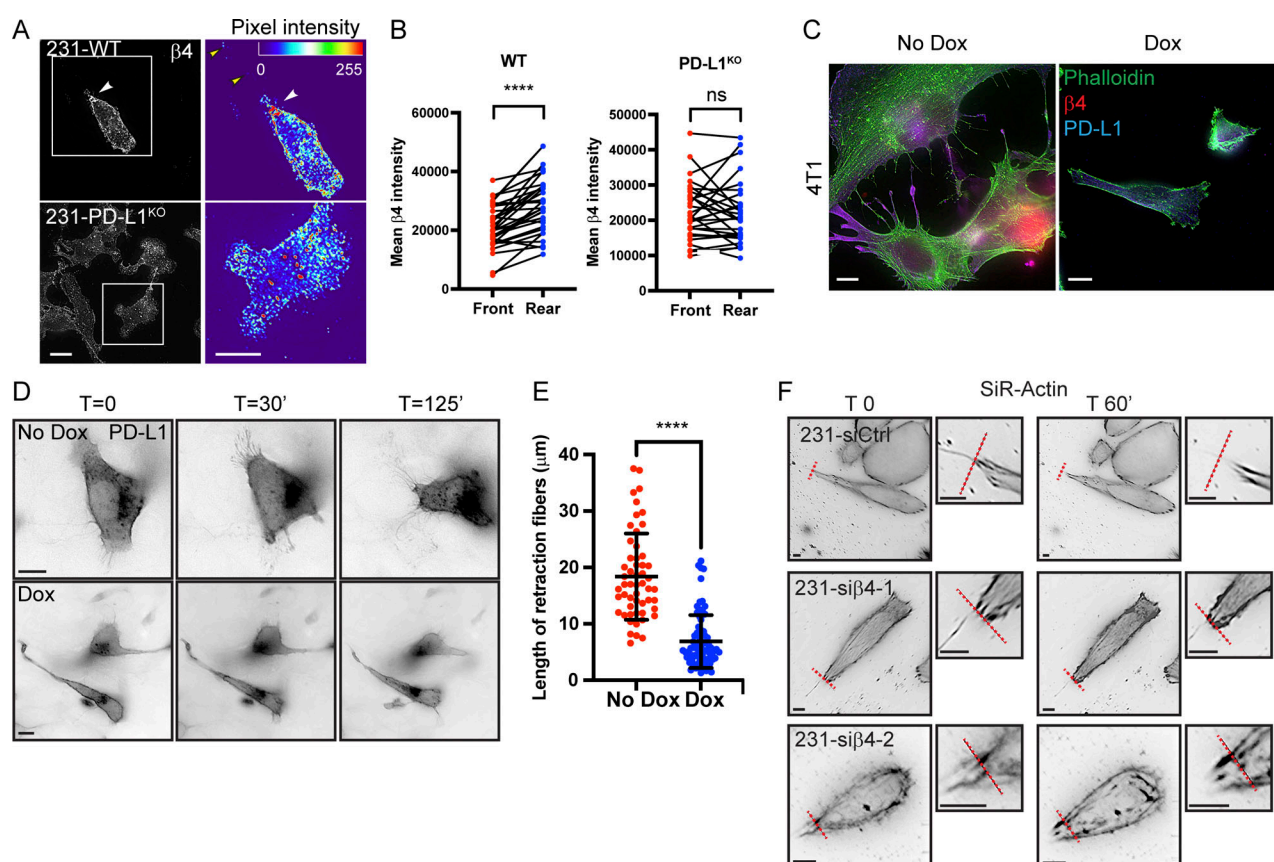
Figure 4. **PD-L1 localizes the β4 integrin to the cell rear, enabling it to facilitate rear retraction and persistent migration. (A)** Representative images of WT (top) or PD-L1[KO] (bottom) MDA-MB-231 cells stained with integrin β4 (β4, white). Scale bar: 10 μm. White arrowhead points to the rear of a migrating cell. Right panels show pixel intensity map of integrin β4 signal from the image in the left panel. Scale bar: 10 μm. White arrowhead points to the rear of a migrating cell. Yellow arrowheads point to migrasome-like structures. **(B)** Quantification of the β4 integrin signal at the front and rear in the same cell in WT or PD-L1[KO] MDA-MB-231 cells. Statistical significance was determined by two-sided, paired t test (n > 30 cells per condition, three independent experiments). ****, $0.0001 > P$. **(C)** Representative images of dox-inducible shβ4 4T1-β4-tdTomato cells show F-actin (phalloidin, green), PD-L1 (blue), and integrin β4 (red) distribution without dox treatment (left, No Dox) or with dox treatment for 3 days at 2 μg/ml (right, Dox). Scale bar: 10 μm. **(D)** Representative time-lapse microscopy images of dox-inducible shβ4 4T1-β4-tdTomato-PD-L1-GEPF cells without dox treatment (top) or dox treatment for 3 days at 2 μg/ml (bottom) show PD-L1 distribution during cell migration. Scale bar: 10 μm. **(E)** Quantification of retraction fiber length from images of dox-inducible shβ4 4T1-β4-tdTomato-PD-L1-EGFP cells with no dox treatment or dox treatment for 3 days at 2 μg/ml. Data are shown as means ± SD from three independent experiments (No dox treatment: n = 54, dox treatment: n = 78). Statistical significance was determined by two-sided, unpaired t test. ****, $0.0001 > P$. **(F)** Representative time-lapse microscopy images of MDA-MB-231 cells treated with siCtrl (top) or siRNAs against β4 integrin (siβ4-1, middle; siβ4-2, bottom) and labeled with SiR-Actin show rear retraction during cell migration. Scale bar: 5 μm. Red dotted lines indicate cell rear.
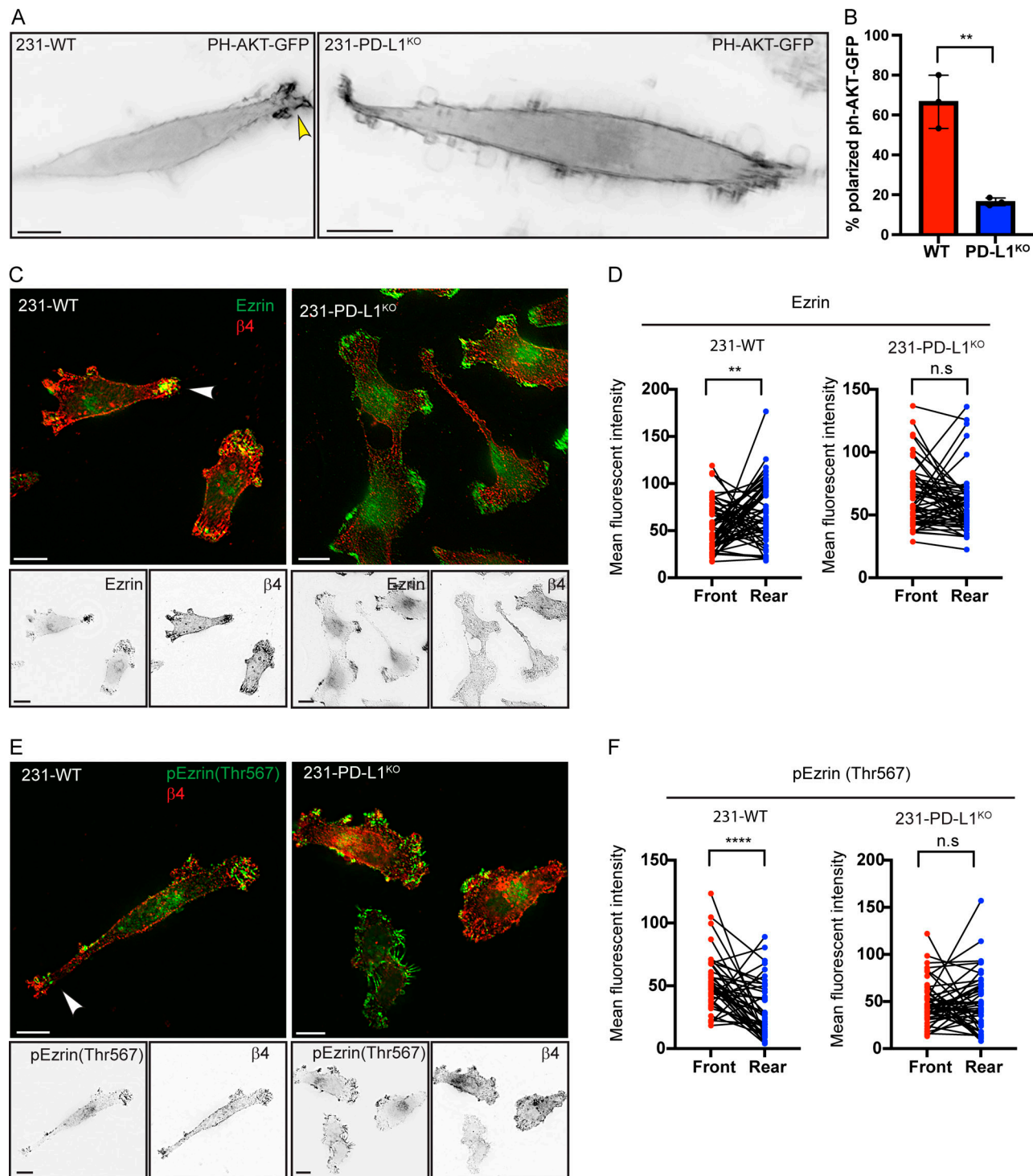
Figure 5. **PD-L1 regulates front-rear polarity in migrating cells. (A)** Fluorescent images of live WT or PD-L1[KO] MDA-MB-231 cells show distribution of PH-AKT-GFP. Arrowhead indicates cell front. Scale bar: 10 μm. **(B)** Quantification of the percentage of cells with polarized distribution of PH-AKT-GFP in WT or PD-L1[KO] MDA-MB-231 cells. Data are shown as means ± SD from three independent experiments. Statistical significance was determined by two-sided, unpaired t test. **, $0.01 > P ≥ 0.001$. **(C)** Representative images show distribution of ezrin (green) and β4 integrin (red) in WT or PD-L1[KO] MDA-MB-231 cells. Single channel only images are shown in black-white images. White arrowhead points to the cell rear. Scale bar: 10 μm. **(D)** Quantification of ezrin signal at the front and rear in the same cell in WT or PD-L1[KO] MDA-MB-231 cells. Statistical significance was determined by two-sided, paired t test ($n > 50$ cells per condition, three independent experiments). **, $0.01 > P ≥ 0.001$. **(E)** Representative images show distribution of p-ezrin (Thr567; green) and β4 integrin (red) in WT or PD-L1[KO] MDA-MB-231 cells. Single-channel only images are shown in black-white images. White arrowhead points to the cell rear. Scale bar: 10 μm. **(F)** Quantification of p-ezrin (Thr567) signal at the front and rear in the same cell in WT or PD-L1[KO] MDA-MB-231 cells. Statistical significance was determined by two-sided, paired t test ($n > 50$ cells per condition, three independent experiments). ****, $0.0001 > P$.

Ezrin is conformationally regulated: a closed inactive conformation in which the N and C termini are tightly bound (Gary and Bretscher, 1995) or an open active conformation that results from binding to phosphatidylinositol 4,5-bisphosphate followed by phosphorylation of the COOH-terminal threonine (T567) (Bretscher et al., 2002; Matsui et al., 1998). In migrating breast cancer cells, p-ezrin is highly polarized at the leading edge (Donatello et al., 2012; Prag et al., 2007). Consistent with these studies, we observed significantly higher p-ezrin (T567) staining at the cell front compared with the rear in WT cells (Fig. 5, E and F). In contrast, PD-L1 knockout cells displayed p-ezrin (T567) staining around the cell periphery (Fig. 5, E and F). Taken together, our data indicate that PD-L1 maintains front–rear polarity. Specifically, it is required to establish a clear cell rear during persistent cell migration.

PD-L1 localizes the β4 integrin to the cell rear by generating a membrane tension gradient

The foregoing data prompted us to investigate how PD-L1 maintains polarity during persistent cell migration. During persistent cell migration, cells establish front–rear polarity by the generation of a membrane tension differential with tension significantly lower at the cell rear than the front (Hetmanski et al., 2019; Houk et al., 2012). p-Ezrin is a major regulator of membrane tension in epithelial cells (Rouven Bruckner et al., 2015) because it links the plasma membrane to the underlying cytoskeleton (Liu et al., 2012; Rouven Bruckner et al., 2015; Sitarska and Diz-Munoz, 2020). Based on our observation that PD-L1 regulates the localization of ezrin and p-ezrin (Fig. 5, C–F), we investigated whether PD-L1 regulates membrane tension. To measure membrane tension in live cells, we used Flipper-TR, a small molecule that intercalates into membranes and indicates in-plane membrane tension through changes in the fluorescence lifetime of the probe (Colom et al., 2018). Higher fluorescence lifetime indicates higher membrane tension (Colom et al., 2018). Indeed, fluorescence lifetime imaging microscopy (FLIM) revealed that the Flipper-TR lifetime increased significantly in the same cell in response to 50% hypo-osmotic shock, a well-documented method that causes cell swelling, to rapidly increase membrane tension (Houk et al., 2012; Le Roux et al., 2019; Sinha et al., 2011; Fig. S4, A and B). We measured the PD-L1 signal in the front and rear of migrating cells (Fig. 6 A, left panel) and quantified Flipper-TR lifetime as a measurement of membrane tension in the same regions to correlate with PD-L1 signal (Fig. 6 A, right panel). Our data show the intensity of the PD-L1 signal correlates with lower membrane tension at the rear of migrating cells (Fig. 6 B). The difference of membrane tension is abolished in cells without PD-L1 (Fig. 6, C and D), suggesting that PD-L1 is required to maintain differential membrane tension between the cell rear and front. We next investigated if low membrane tension is required to concentrate integrin β4 at the rear of migrating cells. To test this hypothesis, live-cell imaging was used to track PD-L1 and β4 integrin localization in migrating cells that were switched from isotonic to hypo-osmotic medium. This change of osmolarity resulted in the rapid movement of PD-L1 and β4 from the rear of the cell toward the inner cell body (Fig. 6, E and F; and Fig. S4 C). Since the β4 integrin was labeled

in live cells using an antibody (439-9B) that recognizes its extracellular domain (Kennel et al., 1990), the signal observed inside the cells at the rear was generated through β4 internalization. Similar results were obtained by labeling PD-L1 with a fluorescent-conjugated antibody and tracking cell migration (Fig. S4 D). In contrast, PD-L1 knockout cells showed no change of β4 distribution upon hypo-osmotic shock with β4 diffusely localized at the plasma membrane while maintaining strong expression in intracellular vesicles, although photo-bleaching of the β4 signal was observed (Fig. 6, G and H). It is unlikely that PD-L1 affects the rate of β4 internalization because PD-L1 knockout did not alter β4 surface or protein expression (Fig. S3, A and B). Taken together, our data indicate that PD-L1 is required to maintain differential membrane tension between cell front and rear and, consequently, localizes the β4 integrin to the rear of the migrating cell.

We next investigated how lower membrane tension localizes β4 at the rear. We were intrigued by the report that this integrin can localize in lipid rafts that are rich in caveolin-1 (Gagnoux-Palacios et al., 2003). Lipid rafts, including planar lipid rafts and caveolae, are microdomains of the cell membrane enriched in cholesterol, sphingomyelin, and glycosylphosphatidylinositol-anchored proteins (Allen et al., 2007). They are associated with the cytoskeleton, resistant to detergent extraction (Allen et al., 2007), and function in cell adhesion and migration (Murai, 2012). Importantly, caveolae, the most readily observed structures associated with lipid rafts (Allen et al., 2007), can function as a plasma membrane sensor (Parton and del Pozo, 2013). In response to increases in membrane tension, caveolae rapidly flatten to supply lipids to the plasma membrane to buffer tension increases directly, rather than through caveolae endocytosis (Le Roux et al., 2019; Sinha et al., 2011). In addition, it was reported that caveolae, marked by the presence of caveolins and confirmed by electron microscopy, form in response to low membrane tension at the cell rear to activate the contractile actin cytoskeleton to promote rapid retraction (Hetmanski et al., 2019). Consistent with these observations, we observed that WT MDA-MB-231 cells expressed significantly more caveolin-1 at the rear of migrating cells than PD-L1 knockout cells (Fig. 6 I). These data prompted us to hypothesize that β4 concentrates at the rear because β4 containing lipid rafts/caveolae form in response to lower membrane tension that is maintained by PD-L1. To address this issue, we used florescent-conjugated cholera toxin subunit B (CT-B) to visualize lipid rafts/caveolae in live cells because it binds to the glycosphingolipid GM1 that selectively partitions into lipid rafts and caveolae (Day and Kenworthy, 2015; Henley et al., 1998; Parton, 1994; Shvets et al., 2015). We observed that PD-L1 and the β4 integrin co-localize with CT-B at the rear of migrating cells (Fig. 6 J), which is consistent with the finding that caveolae form at the cell rear (Hetmanski et al., 2019). Although WT MDA-MB-231 cells showed accumulation of both CT-B and the β4 integrin at the rear of migrating cells (Fig. 6 K), depletion of PD-L1 prevented the polarized localization of CT-B and β4 integrin at the rear (Fig. 6 K). Thus, PD-L1 is required for lipid rafts/caveolae that contain β4 integrin to form at the rear of migrating cells in response to lower membrane tension.
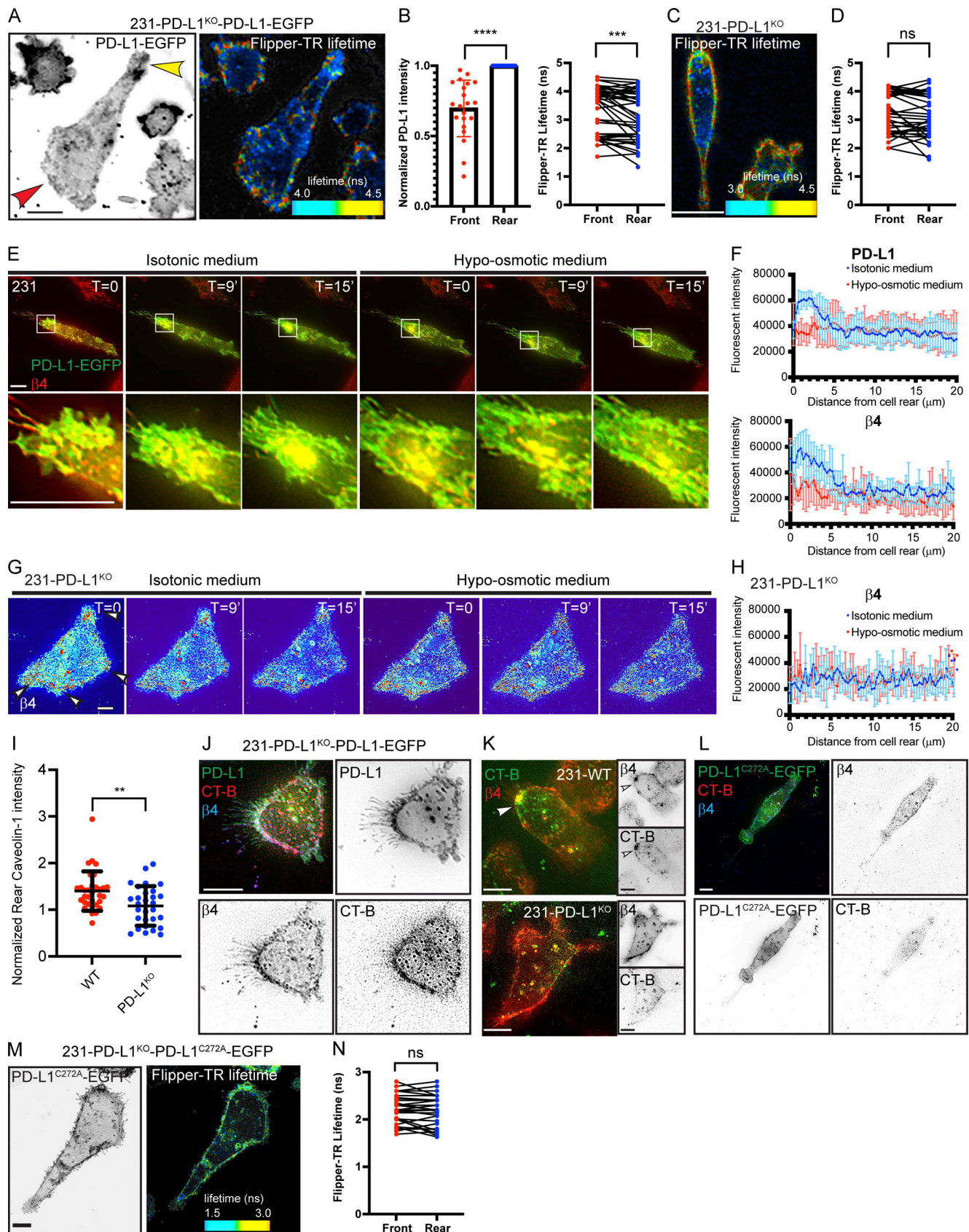
Figure 6. **PD-L1 localizes the β4 integrin to the cell rear by generating a membrane tension gradient. (A)** Left: a representative image of PD-L1-EGFP in a migrating cell. Yellow arrowhead indicates cell rear. Red arrowhead indicates cell front. Right: heat-map images show Flipper-TR lifetime. Scales of lifetime is indicated in rainbow bar. Scale bar: 10 μm. **(B)** Left: Quantification of PD-L1 intensity normalized to the rear of the cell. Data are shown as means ± SD (*n* = 46

cells, three independent experiments). Statistical significance was determined by unpaired *t* test. Right: quantification of Flipper-TR lifetime at the front and rear of the cell. Statistical significance was determined by two-sided, paired *t* test (*n* = 46 cells, three independent experiments). ***, 0.001 > P ≥ 0.0001; ****, 0.0001 > P. **(C)** A Heat-map image showing Flipper-TR lifetime in 231-PD-L1^KO cells. Scale bar: 10 μm. **(D)** Quantification of Flipper-TR lifetime at the front and rear of the cell in 231-PD-L1^KO cells. Statistical significance was determined by two-sided, paired *t* test (*n* = 40 cells, three independent experiments). **(E)** Time-lapse images of PD-L1^KO-PD-L1-EGFP MDA-MB-231 cells in isotonic (left) or hypo-osmotic medium (right). Top: merged images of PD-L1 (green) and integrin β4 (red). Bottom: Higher magnification images of the boxed regions in the top panels. Scale bar: 10 μm. The same images were used to generate the pixel intensity map images shown in Fig. S4 C. **(F)** Quantification of PD-L1 (top) and integrin β4 (bottom) fluorescent intensity correlates with the distance from cell rear in PD-L1^KO-PD-L1-EGFP MDA-MB-231 cells (*n* = 10 cells, three independent experiments). **(G)** Pixel intensity map from time-lapse images of PD-L1^KO-MDA-MB-231 cells in isotonic (left) or hypo-osmotic medium (right) show integrin β4 distribution. White arrowheads indicate location of the integrin β4. Scale bar: 10 μm. **(H)** Quantification of integrin β4 fluorescent intensity correlates with the distance from cell rear in PD-L1^KO-MDA-MB-231 cells (*n* = 10 cells, three independent experiments). **(I)** Quantification of the cell rear caveolin-1 intensity in WT or PD-L1^KO MDA-MB-231 cells. Data are shown as means ± SD from three independent experiments, *n* > 30 cells per condition. Statistical significance was determined by two-sided, unpaired *t* test. **, 0.01 > P ≥ 0.001. **(J)** Fluorescent images of PD-L1^KO-PD-L1-EGFP MDA-MB-231 cells show distribution of PD-L1 (green), integrin β4 (β4, blue), and CT-B (red). Single channel only images are shown in black-white images. Scale bar: 10 μm. **(K)** Fluorescent images of WT (top) or PD-L1^KO (bottom) MDA-MB-231 cells show distribution of CT-B (green) and integrin β4 (β4, red). Single channel only images are shown in black-white images. White arrowhead points to accumulation of caveolae/lipid rafts at the cell rear. Scale bar: 10 μm. **(L)** Fluorescent images of PD-L1^KO-PD-L1^C272A-EGFP MDA-MB-231 cells show distribution of PD-L1^C272A-EGFP (green), CT-B (red), and integrin β4 (blue). Single channel only images are shown in black-white images. Scale bar: 10 μm. **(M)** Left: a representative image of PD-L1^C272A-EGFP in a migrating cell. Right: a heat-map image shows Flipper-TR lifetime. Scales of lifetime is indicated in rainbow bar. Scale bar: 10 μm. **(N)** Quantification of Flipper-TR lifetime at the front and rear of the cell in PD-L1^KO-PD-L1^C272A-EGFP MDA-MB-231 cells. Statistical significance was determined by two-sided, paired *t* test (*n* = 40 cells, three independent experiments).

Given that palmitoylation of proteins promotes their incorporation into lipid rafts (Levental et al., 2010) and that PD-L1 can be palmitoylated (Yang et al., 2019; Yao et al., 2019), we investigated the potential contribution of PD-L1 palmitoylation to the localization of the β4 integrin and rear retraction. We replaced the endogenous PD-L1 in MDA-MB-231 cells with EGFP-tagged PD-L1 mutant with Cys272 substitute to Ala (PD-L1^C272A-EGFP), which abolishes its palmitoylation (Yang et al., 2019; Yao et al., 2019), and analyzed the localization of mutant PD-L1, β4 integrin, and CT-B in the same migrating cell. Like PD-L1 knockout cells (Fig. 4 A), the β4 integrin and CT-B exhibited a diffuse localization on cell surface and in intracellular vesicles in cells that expressed PD-L1^C272A-EGFP mutant (Fig. 6 L). Thus, PD-L1 palmitoylation is required to localize β4 integrin containing caveolae/lipid rafts to the cell rear. In contrast to WT PD-L1, the PD-L1^C272A-EGFP mutant did not concentrate at the rear (Fig. 6 M). Also, cells expressing PD-L1^C272A-EGFP mutant did not exhibit a membrane tension gradient (Fig. 6, M and N), indicating that PD-L1 palmitoylation is required to maintain a front–rear membrane tension gradient. Cells expressing PD-L1^C272A-EGFP mutant showed no difference of retraction fiber length compared with PD-L1 knockout cells and significantly fewer migrasomes/retraction fiber length compared with cells expressing PD-L1^WT-EGFP (Fig. S4 E). Taken together, our data indicate that palmitoylation of PD-L1 maintains a front–rear membrane tension difference that localizes β4 containing caveolae/lipid rafts to the cell rear to promote rear retraction.

PD-L1 promotes rear contractility by enabling the β4 integrin to engage the cytoskeleton and activate RhoA

Next, we investigated the mechanism by which PD-L1 regulates β4 to promote contractility that is required for rear retraction. We reported previously that the β4 integrin can engage the actin cytoskeleton in migrating carcinoma cells and promote the formation of actin-containing protrusions (Rabinovitz and Mercurio, 1997). To assess the possibility that PD-L1 facilitates the association of β4 with F-actin, we extracted live cells in situ with a 0.5% Triton X-100 buffer that removes soluble proteins

but not actin-associated proteins (Capco et al., 1982; Fey et al., 1984). This buffer did not alter the intensity or localization of the β4 signal in WT cells (Fig. 7 A). However, the cell surface β4 signal was abolished in cells with PD-L1 knockout (Fig. 7 A). Expression of PD-L1^WT-EGFP in PD-L1 knockout cells caused the β4 signal to resist detergent extraction while expression of PD-L1^C272A-EGFP mutant did not (Fig. 7 B). These data indicate that PD-L1 promotes the association of β4 with F-actin, a process that is dependent on PD-L1 palmitoylation.

Rear retraction in migrating cells requires activation of RhoA and Rock1, which phosphorylates myosin phosphatase and the regulatory light chain on myosin II to increase actin–myosin contractility (Petrie et al., 2009). Thus, we investigated whether PD-L1 enables the β4 integrin to activate RhoA at the rear to promote contractility. Using a RhoA-EGFP biosensor (EGFP-AHPH; Piekny and Glotzer, 2008), we observed that active RhoA co-localizes with β4 on the membrane at the cell rear in WT cells. Co-localization was less evident on other areas of the plasma membrane (Fig. 7 C). In contrast, RhoA activity was diminished and more diffuse in PD-L1 knockout cells (Fig. 7 D), indicating that PD-L1 contributes to RhoA activation and its localization at the rear. Next, we investigated the contribution of the β4 integrin to RhoA activity using siRNA (Fig. 7 E and Fig. S3 H). Active RhoA was evident at the rear of control siRNA (siCtrl) cells, as well as elsewhere on the membrane (Fig. 7 E), like WT cells (Fig. 7 C). However, membrane localization of active RhoA was abolished in siβ4 cells (Fig. 7 E), indicating that β4 regulates membrane RhoA activity. To substantiate these findings, we used a RhoA fluorescence resonance energy transfer (FRET) biosensor (Raichu-RhoA) to measure RhoA activity (Yoshizaki et al., 2003). RhoA activity was diminished significantly at the cell rear in PD-L1 knockout cells compared with WT cells (Fig. 7, F and G). Similarly, RhoA activity at the cell rear was significantly inhibited in siβ4 cells compared with siCtrl cells (Fig. 7 H). Consistent with these data, phosphorylated myosin light chain (pS19-MLC), which is regulated by RhoA (Kimura et al., 1996), was significantly enriched at cell rear compared with the front in WT cells, but this polarized
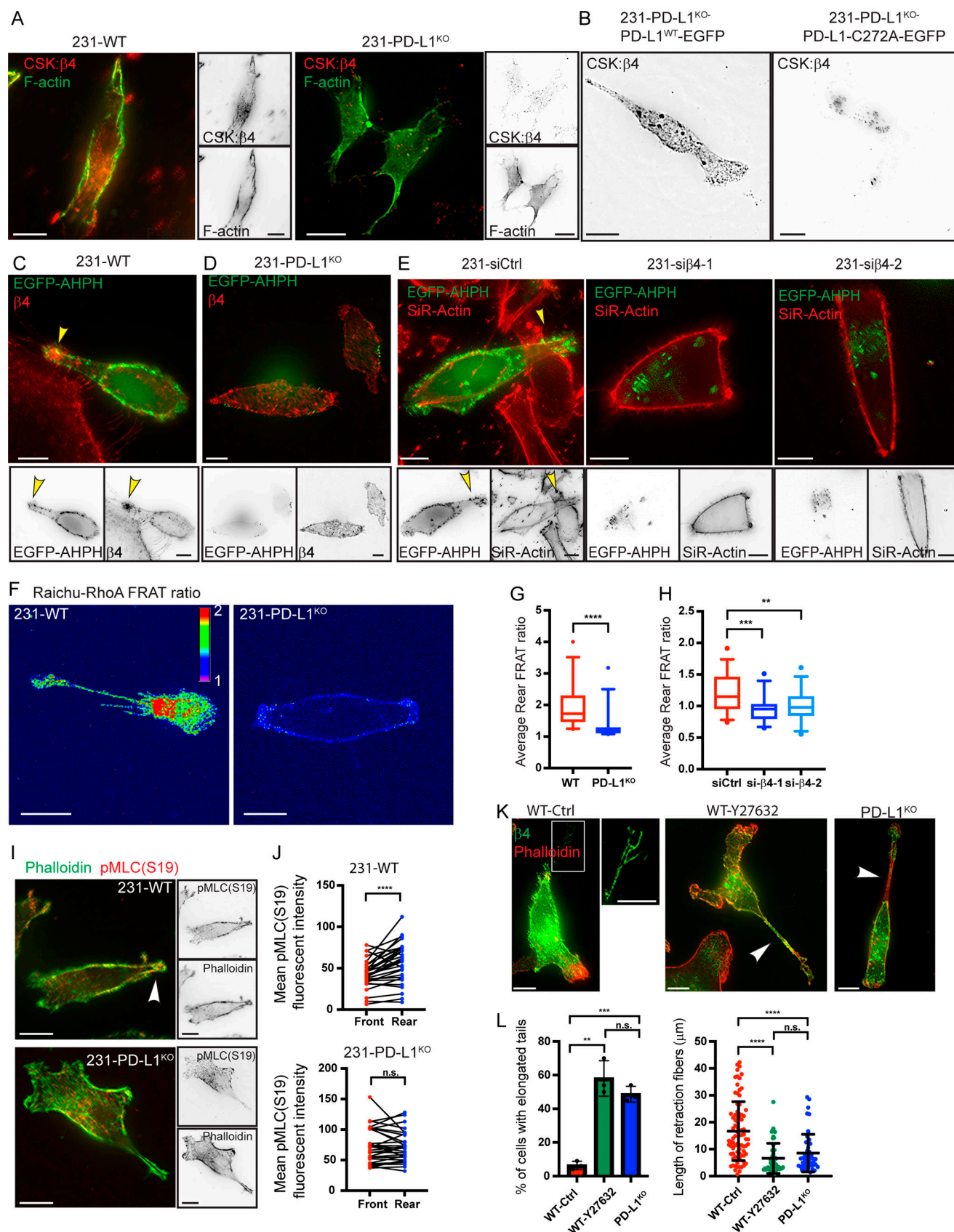
Figure 7. PD-L1 promotes rear contractility by enabling the β4 integrin to engage the cytoskeleton and activate RhoA. (A) Fluorescent images of WT (left) or PD-L1[KO] (right) MDA-MB-231 cells treated with 0.5% Triton X in PBS before fixation show distribution of cytoskeleton-associated integrin β4 (CSK:β4, red), and F-actin (green). Single channel only images are shown in black-white images. Scale bar: 10 μm. **(B)** Fluorescent images of PD-L1[KO]-PD-L1-EGFP (left)

or PD-L1^{KO}-PD-L1^{C272A}-EGFP (right) MDA-MB-231 cells treated with 0.5% Triton X in PBS before fixation show distribution of cytoskeleton associated integrin β4 (CSK:β4). Scale bar: 10 µm. **(C)** Fluorescent images of live WT MDA-MB-231 cells expressing the plasmid of EGFP-AHPH (RhoA Biosensor) show distribution of integrin β4 (red) and activate RhoA (EGFP-AHPH, green). Single-channel only images are shown in black-white images. Arrowheads indicate cell rear. Scale bar: 10 µm. **(D)** Fluorescent images of live PD-L1^{KO} MDA-MB-231 cells expressing the plasmid of EGFP-AHPH (RhoA Biosensor) show distribution of integrin β4 (red) and activate RhoA (EGFP-AHPH, green). Single channel only images are shown in black-white images. Scale bar: 10 µm. **(E)** Fluorescent images of live MDA-MB-231 cells treated with siCtrl (left) or siRNAs against β4 integrin (middle and right) show distribution of F-actin (red) and activate RhoA (EGFP-AHPH, green). Single channel only images are shown in black-white images. Arrowheads indicate cell rear. Scale bar: 10 µm. **(F)** Raichu-RhoA FRET ratio images of WT and PD-L1^{KO} MDA-MB-231 cells. Scale bar: 10 µm. **(G)** Quantification of average rear Raichu-RhoA FRET ratio in WT and PD-L1^{KO} MDA-MB-231 cells. Data are shown as box-whisker plots (5-95 percentile) from three independent experiments, n > 30 cells per condition. Statistical significance was determined by two-sided, unpaired t test. ****, 0.0001 > P. **(H)** Quantification of average rear Raichu-RhoA FRET ratio in MDA-MB-231 cells treated with siCtrl or siRNAs against β4 integrin. Data are shown as box-whisker plots (5-95 percentile) from three independent experiments, n > 30 cells per condition. Statistical significance was determined by two-sided, unpaired t test. **, 0.01 > P ≥ 0.001; ***, 0.001 > P ≥ 0.0001. **(I)** Fluorescent images of WT (top) or PD-L1^{KO} (bottom) MDA-MB-231 cells show distribution of actin (phalloidin, green), and pMLC(S19) (red). Single channel only images are shown in black-white images. White arrowhead points to the cell rear. Scale bar: 10 µm. **(J)** Quantification of pMLC(S19) signal at cell rear and cell front in WT or PD-L1^{KO} MDA-MB-231 cells. Data are shown as before-after plots from three independent experiments, n > 30 cells per condition. Statistical significance was determined by two-sided, paired t test. ****, 0.0001 > P. **(K)** Fluorescent images of MDA-MB-231 cells treated with either H$_2$0 (WT-Ctrl, left) or Y27632 (10 µM for 1 h; middle) were compared with PD-L1^{KO} cells (right) for the distribution of actin (phalloidin, red), and β4 integrin (green). White arrowhead points to elongated tails. Scale bar: 10 µm. **(L)** Quantification of the percentage of MDA-MB-231 cells described in K with elongated tails (left) and the length of their retraction fibers (right). Data are shown as means ± SD from three independent experiments, n > 30 cells per condition. Statistical significance was determined by two-sided, unpaired t test. **, 0.01 > P ≥ 0.001; ***, 0.001 > P ≥ 0.0001; ****, 0.0001 > P.

distribution of pS19-MLC was diminished in response to PD-L1 depletion (Fig. 7, I and J). Moreover, PD-L1 depletion phenocopied treatment with Y27632, which blocks Rho-mediated activation of actomyosin (Uehata et al., 1997; Fig. 7, K and L). Both Y27632 treatment and PD-L1 depletion resulted in significantly more cells with elongated tails (Fig. 7, K and L), a cell-retraction defect phenotype (Worthylake et al., 2001) that results in shorter retraction fibers, as we observed (Fig. 7, K and L). Based on these data and previous findings demonstrating that the β4 integrin can activate RhoA (O'Connor et al., 2000), we conclude that PD-L1 regulates RhoA activity through the β4 integrin.

Discussion

The data reported here reveal an unanticipated function of PD-L1 in persistent cell migration that involves its ability to regulate rear retraction. The essence of this function, which is schematized in Fig. 8, is that PD-L1 regulates cell polarity by maintaining lower membrane tension at the cell rear compared with the leading edge of migrating cells. Consistent with previous studies, we propose that lower membrane tension promotes the formation of caveolae at the rear (Hetmanski et al., 2019), where PD-L1 interacts with the β4 integrin to regulate its association with F-actin. The ability of the β4 integrin to associate with F-actin and activate RhoA has been documented by us previously (O'Connor et al., 2000; Rabinovitz and Mercurio, 1997), and we now propose that these functions can be regulated by PD-L1. The contractility generated by PD-L1/β4 integrin–mediated activation of RhoA increases actomyosin tension. This process facilitates persistent cell migration by stimulating rear retraction and the consequent formation of retraction fibers and migrasomes. These findings highlight a novel cell-autonomous function of PD-L1, and they should stimulate further investigation to understand how PD-L1 regulates membrane tension and the role of caveolae/lipid raft dynamics in this process.

A key finding in this study is that PD-L1 localizes the β4 integrin to the rear of migrating cells and enables this integrin to facilitate RhoA-mediated contractility. This finding is a significant advancement in our understanding of how this integrin promotes the migration of carcinoma cells. As mentioned, previous studies by our group have implicated β4 in directional migration and retraction fiber formation by a mechanism that involves its ability to engage F-actin (Rabinovitz and Mercurio, 1997), but an understanding of how this function of β4 is regulated was lacking. The data we provide here indicate that the ability of PD-L1 to maintain lower membrane tension at the cell rear has a causal role in β4 localization and function. Our data are also consistent with our previous finding implicating β4 in RhoA activation in migrating carcinoma cells (O'Connor et al., 2000), although this study did not investigate a role for β4-mediated RhoA activation in rear contractility as we have done here. An important question that arises from these observations is whether PD-L1 preferentially impacts the function of β4 compared with other integrins. Clearly, we cannot exclude the possibility that PD-L1 regulates the function of other integrins involved in directional migration based on the data we present. However, several lines of evidence support our conclusion that β4 is a preferential target of PD-L1–mediated regulation. The PLA data we provide (Fig. 3, E and F) indicate that β4 interacts significantly more with β4 than with β1 integrins, an observation that is supported by the finding that PD-L1 and β4 can be co-immunoprecipitated in ovarian carcinoma cells (Wang et al., 2018). It is also worth noting our previous finding that there is a spatial segregation of β4 and β1 integrins in retraction fibers (Rabinovitz and Mercurio, 1997), suggesting a division of labor between these integrins in migration that may relate to differential regulation by PD-L1.

The data we provide affirm and extend a previous study on the role of membrane tension in regulating rear retraction during directional cell migration (Hetmanski et al., 2019). This study demonstrated that low membrane tension at the cell rear is a key mechanical feature facilitating persistent cell migration. Decreased membrane tension facilitates the formation of caveolae, which in turn recruit Ect2 to coordinate activation of RhoA and its effectors to promote actomyosin contractility,
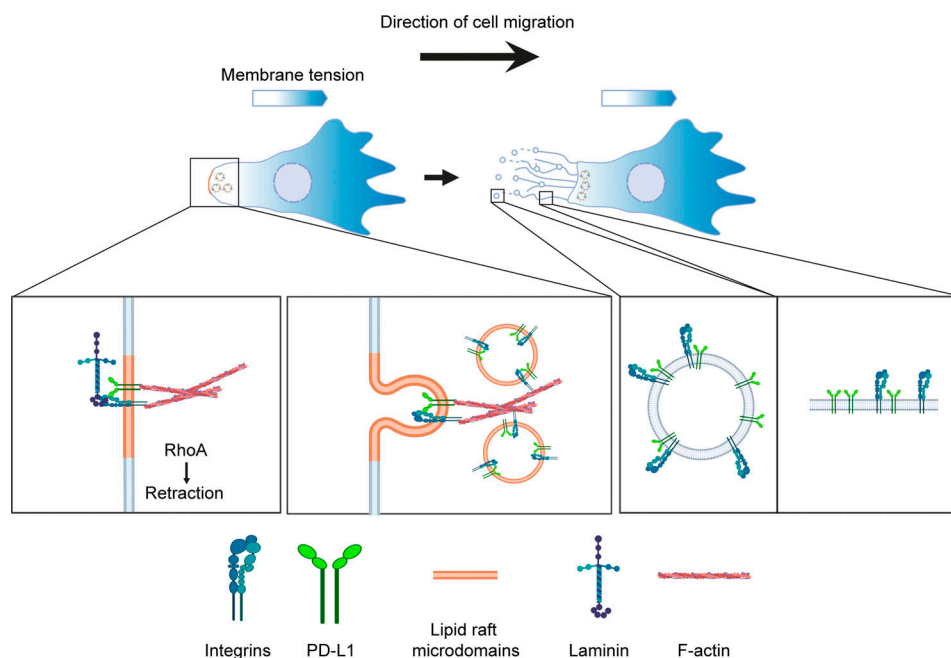
Figure 8. **Schematic of the proposed mechanism for PD-L1 regulation of rear contraction during persistent cell migration.** PD-L1 regulates cell polarity by maintaining lower membrane tension at the cell rear compared with the leading edge of migrating cells. Consequently, caveolae form at the rear where PD-L1 associates with the β4 integrin. This association enables the β4 integrin to associate with F-actin and activate RhoA-mediated contractility that increases actomyosin tension. This process causes rear retraction that results in the formation of PD-L1 and β4 integrin containing retraction fibers and migrasomes. The graph is created with BioRender.com.

establishing positive feedback that sustains low membrane tension, caveolae formation, and hyperactivation of RhoA, resulting in rapid retraction of the migrating cell rear (Hetmanski et al., 2019). Our study advances these findings by demonstrating that PD-L1 is a critical effector of low membrane tension and, consequently, caveolae formation, and that it also enables the β4 integrin to associate with actin at the cell rear to activate RhoA and, consequently, promote rear contractility (Fig. 8). Moreover, the effect of PD-L1 depletion on rear retraction that we observed phenocopies the effects of caveolae depletion reported by Hetmanski et al. (2019) and inhibition of RhoA/ROCK1 (Fig. 7, K and L). These studies reinforce the ability of caveolae to respond to changes in membrane tension, which is consistent with their reported mechanosensing function (Parton and del Pozo, 2013). Caveolae flattening in response to increased membrane tension is reversible and is an inherent property of the caveolar domain that is independent of endocytosis (Sinha et al., 2011). Although the formation of caveolae at the cell rear appears to relate to their ability to form under low membrane tension, it remains possible that caveolae internalization can occur at the cell rear (Hetmanski et al., 2019). Our data suggest that PD-L1 and the β4 integrin are internalized at lipid raft/caveolae-positive foci at the cell rear during migration, and this process is regulated by PD-L1. However, how caveolae undergo endocytosis has been a subject of controversy for many years (Parton and del Pozo, 2013), and whether the internalization of PD-L1 and β4 integrin is required for persistent cell migration remains to be investigated further.

A particularly novel aspect of this study is the localization of PD-L1 and the β4 integrin in migrasomes because it may be important for tumor progression. Cytosolic contents can be released from the migrating cells in migrasomes, a process termed migracytosis (Ma et al., 2015). Also, during zebrafish gastrulation, migrasomes release chemoattractants that enable the correct positioning of cells during organ morphogenesis (Jiang et al., 2019). Thus, PD-L1–containing migrasomes could be internalized by neighboring cells to increase their expression of PD-L1, and they could also release chemokines that facilitate the migration of tumor and stromal cells within the tumor microenvironment. Moreover, the ability of migrasomes generated by invasive cells to release PD-L1 and β4 integrin–containing exosomes could be important for metastasis in light of the report that β4 integrin–containing exosomes promote organotropic metastasis coupled with the potential role of PD-L1 in metastasis (Hoshino et al., 2015). Clearly, the data we report add a new dimension to our understanding of the function of PD-L1 in cell biology and cancer.

Materials and methods
Reagents, antibodies, and cell culture
MDA-MB-231 and 4T1 were obtained from the American Type Culture Collection. All cell lines were maintained at 37°C with 5% CO_2 atmosphere. Compounds were added to and maintained in complete growth medium, unless otherwise specified. All cells were checked quarterly for mycoplasma.

The following antibodies and reagents were used: anti–α-tubulin monoclonal DM1A (62204; Thermo Fisher Scientific), APC anti-human CD274 (B7-H1, PD-L1) antibody (329708; BioLegend), anti-mouse-PD-L1 (ab213480; Abcam), anti-human/

mouse CD274 (PD-L1, B7-H1) monoclonal antibody (MIH1; eBioscience; 14-5983-82; Invitrogen), mouse monoclonal tdTomato antibody, clone OTI2H2 (TA180009; Origene), anti-human CD104 (Integrin β4) monoclonal antibody (439-9B) eFluor 660 eBioscience (50-1049-82; Invitrogen), anti-mouse-Integrin β4 antibody (EPR17517; ab182120; Abcam), anti-human integrin β1 antibody (ZRB1230-25UL; Millpore), anti-human Ezrin antibody (35-7300; Invitrogen), anti-human pEzrin (Thr567; PA5-37763; Invitrogen), anti-GFP antibody (NC97779660; Thermo Fisher Scientific), anti-human integrin β4 Polyclonal Antibody (21738-1-AP; Thermo Fisher Scientific), Alexa Fluor 488 Phalloidin (Invitrogen), SiR-Actin Kit (CY-SC001; Cytoskeleton, Inc.), Vybrant Alexa Fluor 555 Lipid Raft Labeling Kit (V34404; Invitrogen), Flipper-TR (cytoskeleton, CY-SC020), doxycycline hydrochloride (2 µg/ml; Fisher BioReagents), Y-27632 2HCl (selleckchem, S 1049). Secondary antibodies used were as follows: Goat anti-Rabbit IgG (H + L) HRP (32460; Invitrogen), Goat anti-Mouse IgG (H + L) HRP (31430; Invitrogen), Goat anti-Mouse IgG (H + L) Highly Cross-Adsorbed Alexa Fluor Plus 488 secondary antibody (A32723; Invitrogen), and Goat anti-Rabbit IgG (H + L) Highly Cross-Adsorbed Alexa Fluor 555 secondary antibody (A-21429; Invitrogen).

Generation of engineered cell lines

To generate PD-L1 knockout cells, we used Alt-R CRISPR-Cas9 System (IDT). The following gRNAs were used: (Human PD-L1-g1: GGTTCCCAAGGACCTATATG, Human PD-L1-g2: ACAGAGGGCCCGGCTGTTGA, mouse PD-L1-g1: GTTTACTATCACGGCTCCAA, mouse PD-L1-g2: GGGGAGAGCCTCGCTGCCAA). The following reagents were purchased from IDT: Alt-R CRISPR crRNA (2 nmol), CRISPR-Cas9 tracrRNA (Cat. 1072532), and Cas9 Nuclease (Alt-RTM S.p. Cas9 Nuclease 3NLS, Cat. 1074181) and were used to assemble Cas9:crRNA:tracrRNA RNP complex. The RNP complexes were transfected in cells using Nucleofector Device (Amaxa). Pooled PD-L1 negative cells were sorted using flow cytometry following validation of β4 knockout by immunoblotting. Integrin β4 knock-in cells were generated as previously described (Elaimy et al., 2019). In brief, the ms-ITGB4-gRNA (CTGGGGCGCGGGGGAGGTTC) was used to assemble Cas9:crRNA:tracrRNA RNP complex with the same approach above, following transfection with donor plasmid (VectorBuilder ID: VB180312-1325zpa) using Nucleofector Device (Amaxa). Transfected cells were processed for single-cell sorting 72 h later. Cells were clonally expanded and tested with Western blot to detect the tdTomato tag on β4.

To generate cells stably expressing PD-L1^{WT}-EGFP and PD-L1^{C272A}-EGFP, a lentiviral system was used to transduce the cells. The lentiviral plasmid pGIPZ-PD-L1-EGFP (Addgene plasmid #120933) was used (Yang et al., 2018). The lentiviral plasmid for PD-L1^{C272A}-EGFP was purchased from Vector Builder. Lentivirus packaging vectors were obtained from Addgene pMD2.G (plasmid #12259) and psPAX2 (plasmid #12260). Plasmids were cotransfected into HEK-293T cells using Lipofectamine 3000 (cat. L3000008; Thermo Fisher Scientific). Virus was harvested 24 and 48 h after transfection, filtered through 0.45-µm filter, and added to the growth media of cells supplemented with 8 µg/ml polybrene (#H9268; Sigma-Aldrich). Stable cells were selected with 500 ng/ml puromycin for at least 2 wk.

To generate cells stably expressing mCherry-Caveolin or EGFP-AHPH (RhoA-biolsensor), mCherry-Caveolin-C-10 plasmid (plasmid #55008; Addgene) or EGFP-AHPH plasmid (plasmid #68026; Addgene) was transfected into cells using Nucleofector Device (Amaxa), and cells were selected with G418 (500 µg/ml) for 2 wk.

To generate cells expressing RhoA FRET sensor (pCAGGS-Raichu-RhoA-CR) or PH-Akt-GFP, pCAGGS-Raichu-RhoA-CR plasmid (plasmid #40258; Addgene) or PH-Akt-GFP plasmid (plasmid #51465; Addgene) was transfected into cells using Lipofectamine 3000 (cat. L3000008; Thermo Fisher Scientific), and cells were analyzed 24–48 h after transfection.

To generate doxycycline-inducible integrin β4 knock-down cells, the following plasmids were used: SMARTvector Inducible Non-targeting Control (VSC11651; Dharmacon) and a set of 3 SMARTvector Mouse Inducible Itgb4 shRNAs (V3SM11253-230971885: TACAGATCCACGGGGCTCT, V3SM11253-234120085: TACATGTGGGATTGGACCC, and V3SM11253-235886740: TTGGCAAGCAGGCGAACCA). The virus production and transduction were performed as described above. Stable cells were selected with 500 ng/ml puromycin for at least 2 wk.

To transiently knockdown integrin β4 or PD-L1, the following siRNAs from IDT were used: negative control DsiRNA, hs.Ri.ITGB4.13.1: CAGUUCUGCGAGUAUGACAACUUCC, hs.Ri.ITGB4.13.2: CGAGAAGCUUCACACCUAUUUCCCT, hs.Ri.CD274.13.1: GGCAUUGAAUCUACAGAUGUGAGCA, hs.Ri.CD274.13.2: CCUCUGAACAUGAACUGACAUGUCA. The siRNAs were transfected into cells using Lipofectamine 3000 (cat. L3000008; Thermo Fisher Scientific), and cells were analyzed 4 days after transfection.

Flow cytometry

Cells were trypsinized, washed with PBS, and incubated with primary antibodies in complete medium for 1 h at room temperature, followed by PBS washes and a 30-min incubation with secondary antibodies. Cells were washed two times in PBS and fixed with 2% paraformaldehyde in PBS and analyzed using BD LSR IIs flow cytometer (BD Biosciences) and FlowJo (BD).

Immunoblotting

Cells were washed PBS and scraped on ice in radioimmunoprecipitation assay buffer with EDTA and EGTA (BP-115DG; Boston Bioproducts) supplemented with protease and phosphatase inhibitors (04693132001; Roche). Laemmli buffer (BP-111R; Boston Bioproducts) was added to each sample and the lysate was boiled and separated by SDS-PAGE. Nitrocellulose membrane was used for blotting.

Migration assays

Cells were harvested using trypsin, rinsed three times with PBS, and then resuspended in serum-free medium. For migration assays, the lower surface of the membrane in each Transwell chamber (Corning FluoroBlok 24-well plate Permeable Support with 8.0 µm Colored PET Membrane) was coated for 30 min with serum-free medium containing 100 nM LPA. Cells (5×10^4) suspended in serum-free medium were added to the upper chamber. After incubating for 48 h at 37°C, cells that had migrated to the lower surface of the membrane were fixed with 2%

paraformaldehyde and stained with Hoechst 33342 (1:1,000; Invitrogen). Migration was quantified by counting cells per 9 fields using fluorescent microscopy.

Time-lapse microscopy
Cells were grown on 8-well tissue culture Lab-Tek chambered cover glass (Cat# 155411; Thermo Fisher Scientific) in culture medium for imaging. Cells were imaged using a DeltaVision Core system (GE Healthcare Bio-Sciences) equipped with an Olympus IX71 microscope and a cooled charge-coupled CoolSNAP HQ2 camera (Photometrics). The microscope was equipped with temperature and CO_2-controlled environments that maintained an atmosphere of 37°C and 3–5% humidified CO_2. Images were captured every 5 min for 12 h using a 60× Olympus oil (NA 1.42) objective. Images were acquired with softWoRx v1.2 software (Applied Science).

Persistent cell migration assay
This assay was performed using μ-Slide Chemotaxis chamber (IDT, 80326). The cell medium and the μ-Slide were placed into the incubator for equilibration the day before seeding. Before plating cells, the filling ports of the large reservoirs were closed by plugs. Then the filling ports of the side channel were filled with 6 μl of cells at 3×10^6 cells/ml in serum-free medium. Then 6 μl of air was aspirated from the opposite filling ports to flush the cells into the channel followed by closing the two filling ports of the channel. After removing all plugs from the filling ports of the large reservoirs, the slides were incubated in cell culture incubator overnight. Right before imaging samples, both reservoirs were filled with 65 μl serum-free medium followed by filling 2×15 μl 100 nM LPA into one reservoir. The ports were then closed with plugs and the samples were analyzed using time-lapse microscopy as described above. Cells were imaged every 5 min for 12 h. Images were analyzed using free Manual Tracking plugin and Chemotaxis and Migration Tool in ImageJ.

Immunofluorescence microscopy
For fixed cell imaging, cells were cultured on coverslips, washed in PBS, and then fixed in 2% paraformaldehyde in PBS for 20 min at room temperature. After fixation, cells were rinsed with PBS, permeabilized in PBS-0.5% Triton X-100 for 5 min, blocked in blocking buffer (PBS, 5% normal goat serum, 0.1% Triton X-100, and 2 mM NaN_3) for 30 min, and then incubated with primary antibodies in blocking buffer for 1 h at room temperature. Cells were washed three times, 5 min each, in PBS-0.1% Triton X-100, and then incubated with secondary antibodies and Hoechst 33342 (1:1,000; Invitrogen) for 1 h at room temperature. Cells were washed three times, 5 min each, in PBS-0.1% Triton X-100 and mounted in 0.1 M n-propyl gallate, 90% (by volume) glycerol, and 10% PBS solution. Images were taken with a DeltaVision Core system mentioned above using a 60× Olympus oil (NA 1.42) objective. Images were acquired with softWoRx v1.2 software (Applied Science).

Membrane tension measurements by FLIM
Cells cultured on glass-bottom dishes (ibidi #81218-200) were treated with a live-cell imaging medium (1× OptiKlear + 10% FCS) containing 1 mM Flipper TR and incubated at 37°C for 1 h

prior to imaging. Cells were imaged on a Nikon TiE stand with A1 Spectral Detector Confocal and Becker-Hickl TCSPC system with dual SPC-152 control cards, 2 HPM-100-40 detectors, and pulsed lasers (405, 445, 488, 561 nm) connected to the Nikon A1 scan head via port 2 in and auxiliary out. Nikon FLIM module used for data collection in NIS-Elements. The microscope was equipped with temperature and CO_2-controlled environments that maintained an atmosphere of 37°C and 3–5% humidified CO_2. Images were taken using an Apo 60× Oil DIC 1.4 NA objective with 488 nm excitation and 575–625 emission. Following imaging, SPCIMage software (Becker & Hickl) was used to fit fluorescence decay data to a dual exponential model (double fitted photon lifetime histograms), and the lifetime per pixel images were exported. Front and rear of membrane regions were manually identified in the SPCIMage software, and the mean average lifetimes was measured.

FRET
FRET imaging of RhoA activity was performed and quantified as described previously (Hetmanski et al., 2019; Lam et al., 2012). Briefly, randomly chosen Raichu-RhoA expressing cells were captured using a Nikon TiE stand with A1 Spectral Detector Confocal equipped with Nikon DUG-2 4-channel detector unit. Images were taken using an Apo 60× Oil DIC 1.4 NA objective at 37°C. The following three different excitation/emission spectra were captured: Clover donor- Clover donor (Ex 488 nm, Em 525/40), Clover donor- mRuby2 acceptor (Ex 488 nm, Em 600/40), and mRuby2 acceptor-mRuby2 acceptor (Ex 561, Em 600/40). Ratiometric FRET activity was then calculated using NIS-Elements 5.30 software by dividing the donor–acceptor channel by the donor–donor channel. The front and rear of the cell were defined manually based on long-axis identification.

PLA
PLA was performed using Duolink In Situ Red Starter Kit Mouse/Rabbit (DUO92101-1KT; Sigma-Aldrich). Cells were cultured on glass-bottom coverslips and fixed with 2% paraformaldehyde in PBS for 20 min at room temperature. After fixation, cells were rinsed with PBS and permeabilized in PBS-0.5% Triton X-100 for 5 min followed by blocking in Duolink blocking solution for 60 min at 37°C. Then cells were incubated in primary antibodies at 4°C overnight. Then the samples were washed 2×5 min in 1× Wash Buffer A at room temperature followed by incubation with Duolink PLA Probes for 1 h at 37°C. The samples were then washed 2×5 min in 1× Wash Buffer A at room temperature followed by incubation with ligase in the 1× ligation buffer for 30 min at 37°C. After this, the samples were washed 2×5 min in 1× Wash Buffer A at room temperature and then incubated with polymerase in 1× amplification buffer for 100 min at 37°C. Then the samples were washed 2×10 min in 1× Wash Buffer B at room temperature and 0.01× Wash Buffer B for 1 min. Then the samples were mounted using Duolink In Situ Mounting Medium with DAPI. The samples were then imaged as described above.

Hypo-osmotic shock
For live imaging experiments using the hypo-osmotic shock, cells were imaged in isotonic control medium (1× Opti-Klear), as

outlined in the section above, for 15 min using point visiting and capturing at 3-min intervals. The medium was then replaced with 50% 1× Opti-Klear + 50% distilled water, and all cells were subsequently imaged for 15 min in osmotic shock conditions. The same cells were imaged and analyzed in isotonic conditions and osmotic shock conditions.

Statistical analysis

The statistical significance of differences in average measurements was evaluated using two-sided unpaired/paired t tests (GraphPad Prism 9.0). Means are taken to be significantly different if $P < 0.05$. In figures, * indicates $0.05 > P \geq 0.01$, ** indicates $0.01 > P \geq 0.001$, *** indicates $0.001 > P \geq 0.0001$, **** indicates $0.0001 > P$, and ns indicates $P \geq 0.05$ for the indicated pairwise comparison. Error bars in all figures indicate SD.

Online supplemental material

Fig. S1, related to Fig. 1, shows that PD-L1 regulates directional persistent cell migration independently of PD-1. Fig. S2, related to Fig. 3, shows that the engagement of the β4 integrin with laminin-332 contributes to the formation of PD-L1 and β4 integrin-containing retraction fibers. Fig. S3, related to Fig. 3, shows that the β4 integrin regulates cell migration. Fig. S4, related to Fig. 4, shows that PD-L1 regulates membrane tension to localize β4 to the cell rear. Video 1 shows that PD-L1 localizes at retraction fibers and migrasomes in MDA-MB-231 cells. Video 2 shows that PD-L1 localizes at retraction fibers and migrasomes in 4T1 cells. Video 3 shows that PD-L1 WT MDA-MB-231 cells form retraction fibers during cell migration. Video 4 shows that PD-L1 deletion inhibits retraction fiber formation during cell migration. Video 5 shows that PD-L1 and the β4 integrin co-localize at the "roots" of retraction fibers during cell migration. Video 6 shows that control 4T1 cells form PD-L1 containing retraction fibers. Video 7 shows that knock-out of the β4 integrin inhibits retraction fiber formation in 4T1 cells.

Acknowledgments

Author contributions: Conceptualization: M. Wang, A.M. Mercurio; Methodology: M. Wang, C. Xiong, A.M. Mercurio; Software: M. Wang, A.M. Mercurio; Validation: M. Wang, A.M. Mercurio; Formal analysis: M. Wang, A.M. Mercurio; Investigation: M. Wang, A.M. Mercurio; Resources: M. Wang, A.M. Mercurio; Data curation: M. Wang, A.M. Mercurio; Writing—original draft: M. Wang, A.M. Mercurio; Writing—review & editing: M. Wang, A.M. Mercurio; Visualization: M. Wang, A.M. Mercurio; Supervision: M. Wang, A.M. Mercurio; Project administration: M. Wang, A.M. Mercurio; Funding acquisition: A.M. Mercurio, M. Wang.

References

Alam, M.S. 2018. Proximity ligation assay (PLA). *Curr. Protoc. Immunol.* 123: e58. https://doi.org/10.1002/cpim.58

Allen, J.A., R.A. Halverson-Tamboli, and M.M. Rasenick. 2007. Lipid raft microdomains and neurotransmitter signalling. *Nat. Rev. Neurosci.* 8: 128–140. https://doi.org/10.1038/nrn2059

Bretscher, A., K. Edwards, and R.G. Fehon. 2002. ERM proteins and merlin: Integrators at the cell cortex. *Nat. Rev. Mol. Cell Biol.* 3:586–599. https://doi.org/10.1038/nrm882

Capco, D.G., K.M. Wan, and S. Penman. 1982. The nuclear matrix: Three-dimensional architecture and protein composition. *Cell.* 29:847–858. https://doi.org/10.1016/0092-8674(82)90446-9

Chen, L., L. Ma, and L. Yu. 2019. WGA is a probe for migrasomes. *Cell Discov.* 5: 13. https://doi.org/10.1038/s41421-018

Colom, A., E. Derivery, S. Soleimanpour, C. Tomba, M.D. Molin, N. Sakai, M. Gonzalez-Gaitan, S. Matile, and A. Roux. 2018. A fluorescent membrane tension probe. *Nat. Chem.* 10:1118–1125. https://doi.org/10.1038/s41557-018s4150127-3

da Rocha-Azevedo, B., and S.L. Schmid. 2015. Migrasomes: A new organelle of migrating cells. *Cell Res.* 25:1–2. https://doi.org/10.1038/cr.2014.146

Day, C.A., and A.K. Kenworthy. 2015. Functions of cholera toxin B-subunit as a raft cross-linker. *Essays Biochem.* 57:135–145. https://doi.org/10.1042/bse0570135

Donatello, S., I.S. Babina, L.D. Hazelwood, A.D. Hill, I.R. Nabi, and A.M. Hopkins. 2012. Lipid raft association restricts CD44-ezrin interaction and promotion of breast cancer cell migration. *Am. J. Pathol.* 181: 2172–2187. https://doi.org/10.1016/j.ajpath.2012.08.025

Elaimy, A.L., M. Wang, A. Sheel, C.W. Brown, M.R. Walker, J.J. Amante, W. Xue, A. Chan, C.E. Baer, H.L. Goel, and A.M. Mercurio. 2019. Real-time imaging of integrin β4 dynamics using a reporter cell line generated by Crispr/Cas9 genome editing. *J. Cell Sci.* 132:jcs231241. https://doi.org/10.1242/jcs.231241

Fey, E.G., K.M. Wan, and S. Penman. 1984. Epithelial cytoskeletal framework and nuclear matrix-intermediate filament scaffold: Three-dimensional organization and protein composition. *J. Cell Biol.* 98:1973–1984. https://doi.org/10.1083/jcb.98.6.1973

Gagnoux-Palacios, L., M. Dans, W. van't Hof, A. Mariotti, A. Pepe, G. Meneguzzi, M.D. Resh, and F.G. Giancotti. 2003. Compartmentalization of integrin α6β4 signaling in lipid rafts. *J. Cell Biol.* 162:1189–1196. https://doi.org/10.1083/jcb.200305006

Gary, R., and A. Bretscher. 1995. Ezrin self-association involves binding of an N-terminal domain to a normally masked C-terminal domain that includes the F-actin binding site. *Mol. Biol. Cell.* 6:1061–1075. https://doi.org/10.1091/mbc.6.8.1061

Henley, J.R., E.W. Krueger, B.J. Oswald, and M.A. McNiven. 1998. Dynamin-mediated internalization of caveolae. *J. Cell Biol.* 141:85–99. https://doi.org/10.1083/jcb.141.1.85

Hetmanski, J.H.R., H. de Belly, I. Busnelli, T. Waring, R.V. Nair, V. Sokleva, O. Dobre, A. Cameron, N. Gauthier, C. Lamaze, et al. 2019. Membrane tension orchestrates rear retraction in matrix-directed cell migration. *Dev. Cell.* 51:460–475.e10. https://doi.org/10.1016/j.devcel.2019.09.006

Hoshino, A., B. Costa-Silva, T.L. Shen, G. Rodrigues, A. Hashimoto, M. Tesic Mark, H. Molina, S. Kohsaka, A. Di Giannatale, S. Ceder, et al. 2015. Tumour exosome integrins determine organotropic metastasis. *Nature.* 527:329–335. https://doi.org/10.1038/nature15756

Hou, J., R. Zhao, W. Xia, C.W. Chang, Y. You, J.M. Hsu, L. Nie, Y. Chen, Y.C. Wang, C. Liu, et al. 2020. PD-L1-mediated gasdermin C expression switches apoptosis to pyroptosis in cancer cells and facilitates tumour necrosis. *Nat. Cell Biol.* 22:1264–1275. https://doi.org/10.1038/s41556-020-0575-z

Houk, A.R., A. Jilkine, C.O. Mejean, R. Boltyanskiy, E.R. Dufresne, S.B. An-
genent, S.J. Altschuler, L.F. Wu, and O.D. Weiner. 2012. Membrane
tension maintains cell polarity by confining signals to the leading edge
during neutrophil migration. Cell. 148:175–188. https://doi.org/10.1016/j
.cell.2011.10.050

Jiang, D., Z. Jiang, D. Lu, X. Wang, H. Liang, J. Zhang, Y. Meng, Y. Li, D. Wu, Y.
Huang, et al. 2019. Migrasomes provide regional cues for organ mor-
phogenesis during zebrafish gastrulation. Nat. Cell Biol. 21:966–977.
https://doi.org/10.1038/s41556-019-s4150358-6

Kamakura, S., M. Nomura, J. Hayase, Y. Iwakiri, A. Nishikimi, R. Takayanagi,
Y. Fukui, and H. Sumimoto. 2013. The cell polarity protein mInsc reg-
ulates neutrophil chemotaxis via a noncanonical G protein signaling
pathway. Dev. Cell. 26:292–302. https://doi.org/10.1016/j.devcel.2013.06
.008

Kennel, S.J., R.G. Epler, T.K. Lankford, L.J. Foote, V. Dickas, M. Canamucio, R.
Cavalierie, M. Cosimelli, I. Venturo, R. Falcioni, et al. 1990. Second
generation monoclonal antibodies to the human integrin alpha 6 beta 4.
Hybridoma. 9:243–255. https://doi.org/10.1089/hyb.1990.9.243

Kimura, K., M. Ito, M. Amano, K. Chihara, Y. Fukata, M. Nakafuku, B. Ya-
mamori, J. Feng, T. Nakano, K. Okawa, et al. 1996. Regulation of myosin
phosphatase by Rho and Rho-associated kinase (Rho-kinase). Science.
273:245–248. https://doi.org/10.1126/science.273.5272.245

Laganenka, L., R. Colin, and V. Sourjik. 2016. Chemotaxis towards auto-
inducer 2 mediates autoaggregation in Escherichia coli. Nat. Commun. 7:
12984. https://doi.org/10.1038/ncomms12984

Lam, A.J., F. St-Pierre, Y. Gong, J.D. Marshall, P.J. Cranfill, M.A. Baird, M.R.
McKeown, J. Wiedenmann, M.W. Davidson, M.J. Schnitzer, et al. 2012.
Improving FRET dynamic range with bright green and red fluorescent
proteins. Nat. Methods. 9:1005–1012. https://doi.org/10.1038/nmeth
.2171

Le Roux, A.L., X. Quiroga, N. Walani, M. Arroyo, and P. Roca-Cusachs. 2019.
The plasma membrane as a mechanochemical transducer. Philos. Trans.
R. Soc. Lond. B Biol. Sci. 374:20180221. https://doi.org/10.1098/rstb.2018
.0221

Levental, I., D. Lingwood, M. Grzybek, U. Coskun, and K. Simons. 2010.
Palmitoylation regulates raft affinity for the majority of integral raft
proteins. Proc. Natl. Acad. Sci. USA. 107:22050–22054. https://doi.org/10
.1073/pnas.1016184107

Liu, Y., N.V. Belkina, C. Park, R. Nambiar, S.M. Loughhead, G. Patino-Lopez,
K. Ben-Aissa, J.J. Hao, M.J. Kruhlak, H. Qi, et al. 2012. Constitutively
active ezrin increases membrane tension, slows migration, and impedes
endothelial transmigration of lymphocytes in vivo in mice. Blood. 119:
445–453. https://doi.org/10.1182/blood-2011b07-368860

Lorentzen, A., J. Bamber, A. Sadok, I. Elson-Schwab, and C.J. Marshall. 2011.
An ezrin-rich, rigid uropod-like structure directs movement of amoe-
boid blebbing cells. J. Cell Sci. 124:1256–1267. https://doi.org/10.1242/jcs
.074849

Ma, L., Y. Li, J. Peng, D. Wu, X. Zhao, Y. Cui, L. Chen, X. Yan, Y. Du, and L. Yu.
2015. Discovery of the migrasome, an organelle mediating release of
cytoplasmic contents during cell migration. Cell Res. 25:24–38. https://
doi.org/10.1038/cr.2014.135

Matsui, T., M. Maeda, Y. Doi, S. Yonemura, M. Amano, K. Kaibuchi, S. Tsu-
kita, and S. Tsukita. 1998. Rho-kinase phosphorylates COOH-terminal
threonines of ezrin/radixin/moesin (ERM) proteins and regulates their
head-to-tail association. J. Cell Biol. 140:647–657. https://doi.org/10
.1083/jcb.140.3.647

Meili, R., C. Ellsworth, S. Lee, T.B. Reddy, H. Ma, and R.A. Firtel. 1999.
Chemoattractant-mediated transient activation and membrane locali-
zation of Akt/PKB is required for efficient chemotaxis to cAMP in
Dictyostelium. EMBO J. 18:2092–2105. https://doi.org/10.1093/emboj/18
.8.2092

Mercurio, A.M., I. Rabinovitz, and L.M. Shaw. 2001. The alpha 6 beta 4 in-
tegrin and epithelial cell migration. Curr. Opin. Cell Biol. 13:541–545.
https://doi.org/10.1016/s0955-0674(00)00249-0

Murai, T. 2012. The role of lipid rafts in cancer cell adhesion and migration.
Int. J. Cell Biol. 2012:763283. https://doi.org/10.1155/2012/763283

O'Connor, K.L., B.K. Nguyen, and A.M. Mercurio. 2000. RhoA function in
lamellae formation and migration is regulated by the α6β4 integrin and
cAMP metabolism. J. Cell Biol. 148:253–258. https://doi.org/10.1083/jcb
.148.2.253

Olguin-Olguin, A., A. Aalto, B. Maugis, A. Boquet-Pujadas, D. Hoffmann, L.
Ermlich, T. Betz, N.S. Gov, M. Reichman-Fried, and E. Raz. 2021.
Chemokine-biased robust self-organizing polarization of migrating
cells in vivo. Proc. Natl. Acad. Sci. USA. 118:e2018480118. https://doi.org/
10.1073/pnas.2018480118

Parton, R.G. 1994. Ultrastructural localization of gangliosides; GM1 is con-
centrated in caveolae. J. Histochem. Cytochem. 42:155–166. https://doi
.org/10.1177/42.2.8288861

Parton, R.G., and M.A. del Pozo. 2013. Caveolae as plasma membrane sensors,
protectors and organizers. Nat. Rev. Mol. Cell Biol. 14:98–112. https://doi
.org/10.1038/nrm3512

Petrie, R.J., A.D. Doyle, and K.M. Yamada. 2009. Random versus directionally
persistent cell migration. Nat. Rev. Mol. Cell Biol. 10:538–549. https://doi
.org/10.1038/nrm2729

Piekny, A.J., and M. Glotzer. 2008. Anillin is a scaffold protein that links
RhoA, actin, and myosin during cytokinesis. Curr. Biol. 18:30–36.
https://doi.org/10.1016/j.cub.2007.11.068

Prag, S., M. Parsons, M.D. Keppler, S.M. Ameer-Beg, P. Barber, J. Hunt, A.J.
Beavil, R. Calvert, M. Arpin, B. Vojnovic, and T. Ng. 2007. Activated
ezrin promotes cell migration through recruitment of the GEF Dbl to
lipid rafts and preferential downstream activation of Cdc42. Mol. Biol.
Cell. 18:2935–2948. https://doi.org/10.1091/mbc.e06-11-1031

Rabinovitz, I., and A.M. Mercurio. 1997. The integrin α6β4 functions in
carcinoma cell migration on laminin-1 by mediating the formation and
stabilization of actin-containing motility structures. J. Cell Biol. 139:
1873–1884. https://doi.org/10.1083/jcb.139.7.1873

Ridley, A.J., M.A. Schwartz, K. Burridge, R.A. Firtel, M.H. Ginsberg, G. Borisy, J.T.
Parsons, and A.R. Horwitz. 2003. Cell migration: Integrating signals from
front to back. Science. 302:1704–1709. https://doi.org/10.1126/science.1092053

Rouven Bruckner, B., A. Pietuch, S. Nehls, J. Rother, and A. Janshoff. 2015.
Ezrin is a major regulator of membrane tension in epithelial cells. Sci.
Rep. 5:14700. https://doi.org/10.1038/srep14700

Servant, G., O.D. Weiner, P. Herzmark, T. Balla, J.W. Sedat, and H.R. Bourne.
2000. Polarization of chemoattractant receptor signaling during neutro-
phil chemotaxis. Science. 287:1037–1040. https://doi.org/10.1126/science
.287.5455.1037

Shvets, E., V. Bitsikas, G. Howard, C.G. Hansen, and B.J. Nichols. 2015. Dy-
namic caveolae exclude bulk membrane proteins and are required for
sorting of excess glycosphingolipids. Nat. Commun. 6:6867. https://doi
.org/10.1038/ncomms7867

Sinha, B., D. Koster, R. Ruez, P. Gonnord, M. Bastiani, D. Abankwa, R.V. Stan,
G. Butler-Browne, B. Vedie, L. Johannes, et al. 2011. Cells respond to
mechanical stress by rapid disassembly of caveolae. Cell. 144:402–413.
https://doi.org/10.1016/j.cell.2010.12.031

Sitarska, E., and A. Diz-Munoz. 2020. Pay attention to membrane tension:
Mechanobiology of the cell surface. Curr. Opin. Cell Biol. 66:11–18.
https://doi.org/10.1016/j.ceb.2020.04.001

Uehata, M., T. Ishizaki, H. Satoh, T. Ono, T. Kawahara, T. Morishita, H.
Tamakawa, K. Yamagami, J. Inui, M. Maekawa, and S. Narumiya. 1997.
Calcium sensitization of smooth muscle mediated by a Rho-associated
protein kinase in hypertension. Nature. 389:990–994. https://doi.org/10
.1038/40187

Wang, M., J.P. Hinton, J.M.C. Gard, J.G.N. Garcia, B.S. Knudsen, R.B. Nagle,
and A.E. Cress. 2019. Integrin α6β4E variant is associated with actin and
CD9 structures and modifies the biophysical properties of cell–cell and
cell-extracellular matrix interactions. Mol. Biol. Cell. 30:838–850.
https://doi.org/10.1091/mbc.E18-10-0652

Wang, S., J. Li, J. Xie, F. Liu, Y. Duan, Y. Wu, S. Huang, X. He, Z. Wang, and X.
Wu. 2018. Programmed death ligand 1 promotes lymph node metastasis
and glucose metabolism in cervical cancer by activating integrin β4/
SNAI1/SIRT3 signaling pathway. Oncogene. 37:4164–4180. https://doi
.org/10.1038/s41388-018s4130252-x

Worthylake, R.A., S. Lemoine, J.M. Watson, and K. Burridge. 2001. RhoA is
required for monocyte tail retraction during transendothelial migra-
tion. J. Cell Biol. 154:147–160. https://doi.org/10.1083/jcb.200103048

Wu, D., Y. Xu, T. Ding, Y. Zu, C. Yang, and L. Yu. 2017. Pairing of integrins
with ECM proteins determines migrasome formation. Cell Res. 27:
1397–1400. https://doi.org/10.1038/cr.2017.108

Yang, J., J.M. Hsu, H. Sun, L.C. Chan, C.W. Li, J.L. Hsu, Y. Wei, W. Xia, J. Hou, Y. Qiu,
and M.C. Hung. 2019. Palmitoylation stabilizes PD-L1 to promote breast tu-
mor growth. Cell Res. 29:83–86. https://doi.org/10.1038/s41422-018s4140124-5

Yang, Y., C.W. Li, L.C. Chan, Y. Wei, J.M. Hsu, W. Xia, J.H. Cha, J. Hou, J.L.
Hsu, L. Sun, and M.C. Hung. 2018. Exosomal PD-L1 harbors active de-
fense function to suppress T cell killing of breast cancer cells and
promote tumor growth. Cell Res. 28:862–864. https://doi.org/10.1038/
s41422-018s4140060-4

Yao, H., J. Lan, C. Li, H. Shi, J.P. Brosseau, H. Wang, H. Lu, C. Fang, Y. Zhang,
L. Liang, et al. 2019. Inhibiting PD-L1 palmitoylation enhances T-cell
immune responses against tumours. Nat. Biomed. Eng. 3:306–317.
https://doi.org/10.1038/s41551-019-0375-6

Yoshizaki, H., Y. Ohba, K. Kurokawa, R.E. Itoh, T. Nakamura, N. Mochizuki, K. Nagashima, and M. Matsuda. 2003. Activity of Rho-family GTPases during cell division as visualized with FRET-based probes. *J. Cell Biol.* 162:223–232. https://doi.org/10.1083/jcb.200212049

Yu, J., B. Qin, A.M. Moyer, S. Nowsheen, X. Tu, H. Dong, J.C. Boughey, M.P. Goetz, R. Weinshilboum, Z. Lou, and L. Wang. 2020a. Regulation of sister chromatid cohesion by nuclear PD-L1. *Cell Res.* 30:590–601. https://doi.org/10.1038/s41422-020-0315-8

Yu, W., Y. Hua, H. Qiu, J. Hao, K. Zou, Z. Li, S. Hu, P. Guo, M. Chen, S. Sui, et al. 2020b. PD-L1 promotes tumor growth and progression by activating WIP and beta-catenin signaling pathways and predicts poor prognosis in lung cancer. *Cell Death Dis.* 11:506. https://doi.org/10.1038/s41419-020

Zengel, P., A. Nguyen-Hoang, C. Schildhammer, R. Zantl, V. Kahl, and E. Horn. 2011. μ-Slide chemotaxis: A new chamber for long-term chemotaxis studies. *BMC Cell Biol.* 12:21. https://doi.org/10.1186/1471-2121-12-21

Zou, W., J.D. Wolchok, and L. Chen. 2016. PD-L1 (B7-H1) and PD-1 pathway blockade for cancer therapy: Mechanisms, response biomarkers, and combinations. *Sci. Transl Med.* 8:328rv4. https://doi.org/10.1126/scitranslmed.aad7118
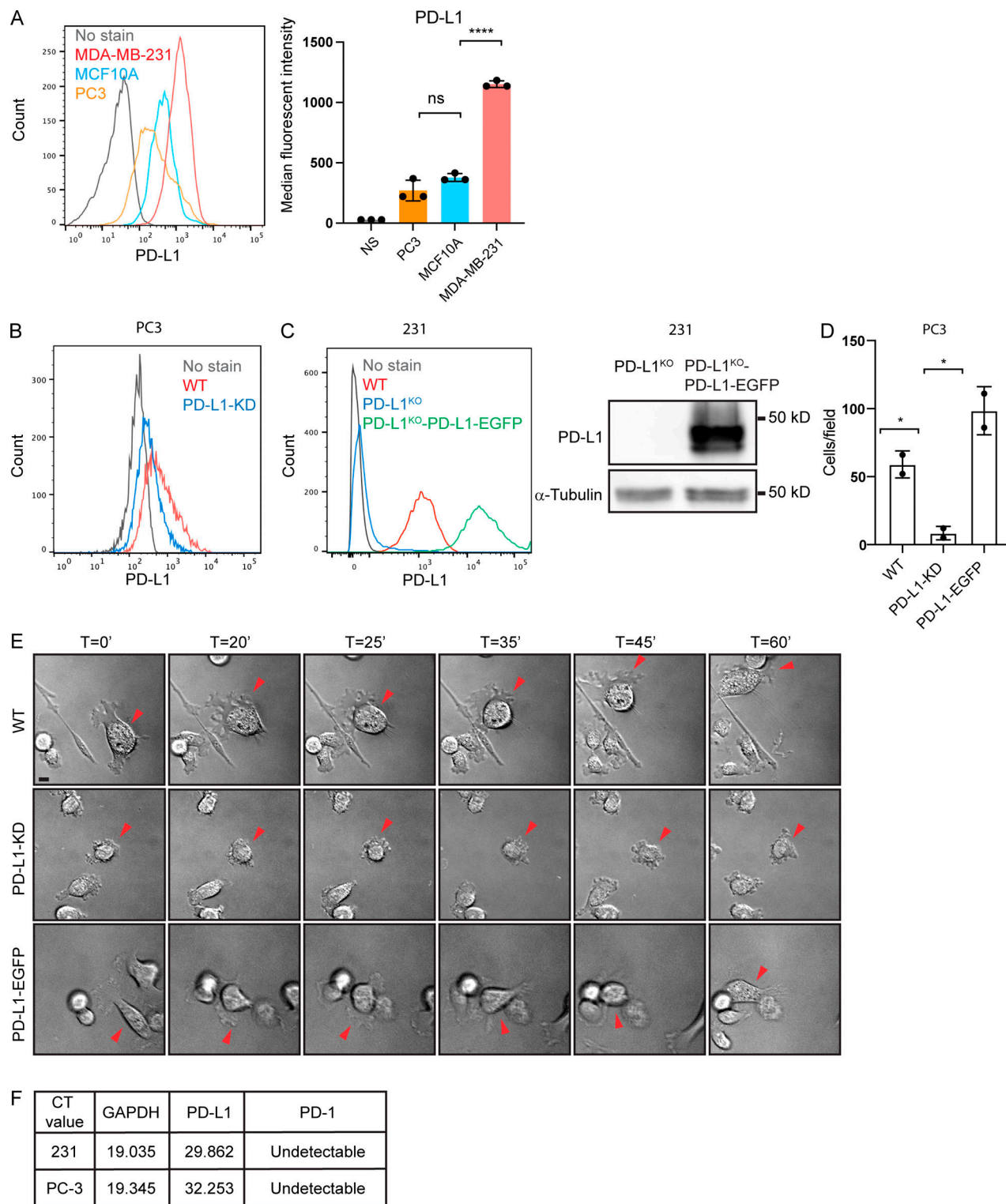
Supplemental material

Figure S1. **PD-L1 regulates directional persistent cell migration independently of PD-1.** Related to Fig. 1. **(A)** Flow cytometry and quantification of cell surface PD-L1 in MCF-10A, PC3, and MDA-MB-231 cells. Data are shown as means ± SD from three independent experiments. Statistical significance was determined by two-sided unpaired t test. ****, $0.0001 > P$. **(B)** Flow cytometry of cell surface PD-L1 in WT and PD-L1^{KO} PC3 cells. **(C)** Left: Flow cytometry of cell surface PD-L1 in PD-L1^{KO} and PD-L1^{KO}-PD-L1-EGFP MDA-MB-231. Right: PD-L1 expression was depleted in MDA-MB-231 and restored by expressing PD-L1-EGFP and protein levels were compared by immunoblotting. **(D)** Trans-well migration assays comparing cell migration in WT, PD-L1^{KD}, and PD-L1-EGFP expressing PC3 cells. Data are shown as means ± SD from three independent experiments. Statistical significance was determined by two-sided unpaired t test. *, $0.05 > P ≥ 0.01$. **(E)** Representative images of WT, PD-L1^{KD}, and PD-L1-EGFP PC3 cells during migration. Arrowheads track individual cell movements. Scale bars: 10 µm. **(F)** Threshold Cycle (CT) value from quantitative PCR results detecting the mRNA expression of GAPDH, PD-L1, and PD-1 in PC3 and MDA-MB-231 cells. Source data are available for this figure: SourceData FS1.
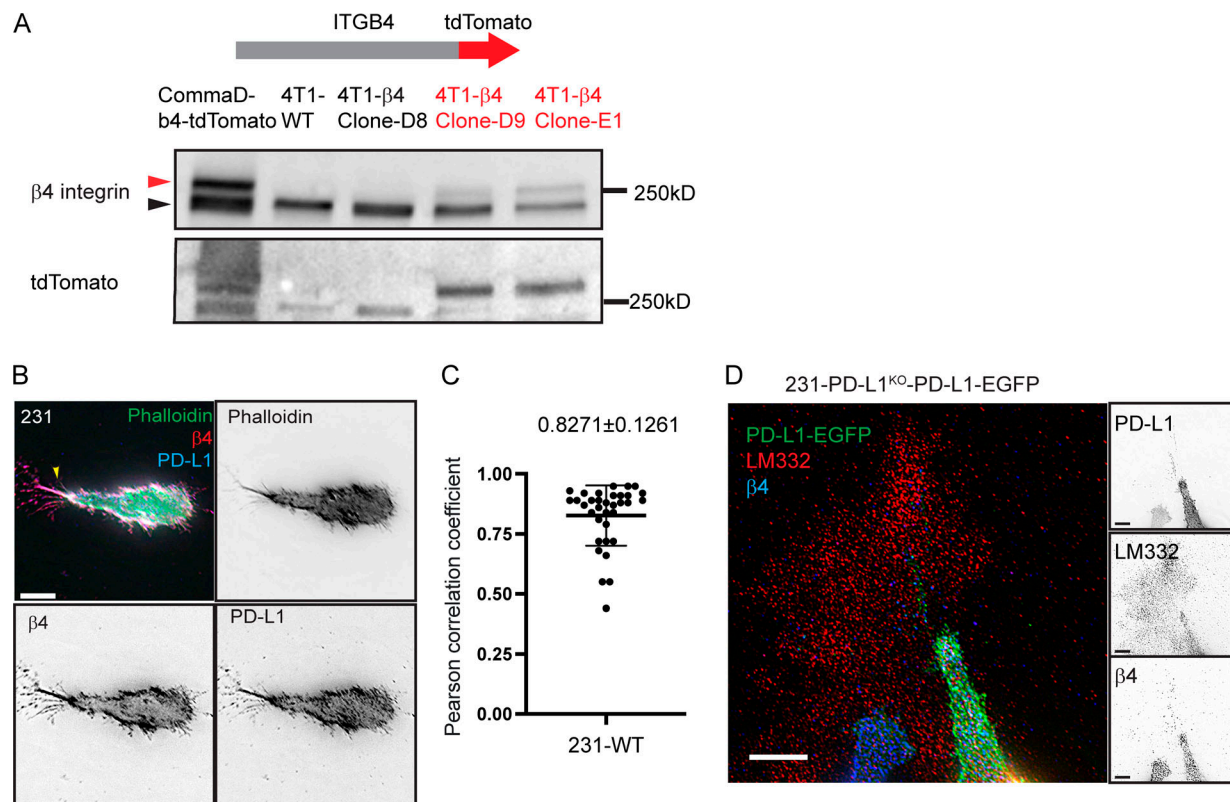
Figure S2. **The engagement of the β4 integrin with laminin-332 contributes to the formation of PD-L1 and β4 integrin containing retraction fibers.** Related to Fig. 3. **(A)** The endogenous β4 integrin was tagged with tdTomato using CRISPR/Cas9. The protein expression of β4-tdTomato was validated by immunoblotting. Red arrowhead shows tagged version of the β4 integrin. **(B)** A representative image of WT MDA-MB-231 cells stained with F-actin (phalloidin, green), integrin β4 (β4, red), and PD-L1 (blue). Arrowhead points to F-actin containing protrusions. Scale bar: 10 µm. **(C)** Quantification of co-localization of PD-L1 and β4 integrin at the actin containing protrusions using Pearson correlation coefficient R value. Data are shown as means ± SD from three independent experiments, n = 34 cells. **(D)** Representative images of PD-L1^{KO}-PD-L1-EGFP MDA-MB-231 cells show merged images (left) of PD-L1 (green), laminin-332 (red), and integrin β4 (blue) distribution. Single channel only images are shown on the right. Scale bar: 10 µm. Source data are available for this figure: SourceData FS2.
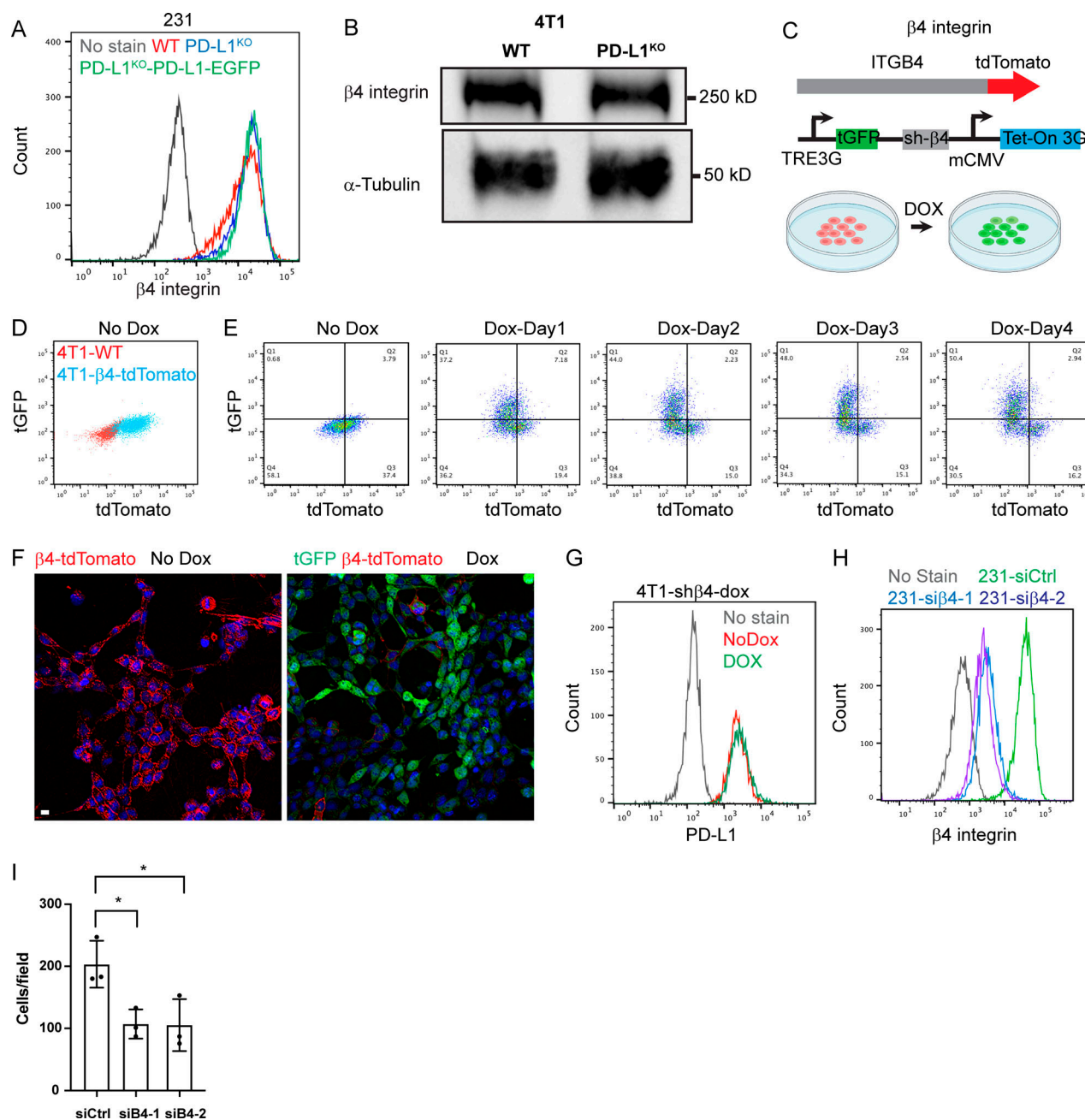
Wang et al.
PD-LI regulates persistent migration

Journal of Cell Biology   S3
https://doi.org/10.1083/jcb.202108083

Figure S3. The β4 integrin regulates cell migration. Related to Fig. 3. **(A)** Flow cytometry of cell surface β4 integrin in WT, PD-L1^KO, and PD-L1^KO-PD-L1-EGFP MDA-MB-231 cells. **(B)** Immunoblotting shows integrin β4 protein expression in WT and PD-L1^KO 4T1 cells. α-Tubulin was used as loading control. The same α-tubulin immunoblot is shown in Fig. 1 A. **(C)** Schematic of the design to generate dox-inducible β4 4T1-β4-tdTomato cells. tGFP, turbo GFP; mCMV, murine cytomegalovirus promoter. **(D)** Flow cytometry of cell surface β4-tdTomato in WT and 4T1-β4-tdTomato cells. **(E)** Flow cytometry of cell surface β4-tdTomato (x-axis) and tGFP (y-axis) in 4T1-β4-tdTomato cells that were treated with doxycycline for different days. **(F)** Representative images of dox-inducible shβ4 4T1-β4-tdTomato cells show β4-tdTomato (red) and tGFP (green) distribution without dox treatment (left, No Dox) or with dox treatment for 3 days at 2 µg/ml (right, Dox). Scale bar: 10 µm. **(G)** Flow cytometry of cell surface PD-L1 in 4T1-β4-tdTomato cells (No Dox, red) or with dox treatment for 3 days at 2 µg/ml (DOX, green). **(H)** Flow cytometry of cell surface β4 integrin in WT MDA-MB-231 cells treated with siCtrl or siRNAs against β4 integrin (siβ4-1 and siβ4-2) for 3 days. **(I)** Trans-well migration assays comparing cell migration in siCtrl and siβ4 MDA-MB-231. Data are shown as means ± SD from three independent experiments. Statistical significance was determined by two-sided unpaired t test. *, 0.05 > P ≥ 0.01. Source data are available for this figure: SourceData FS3.
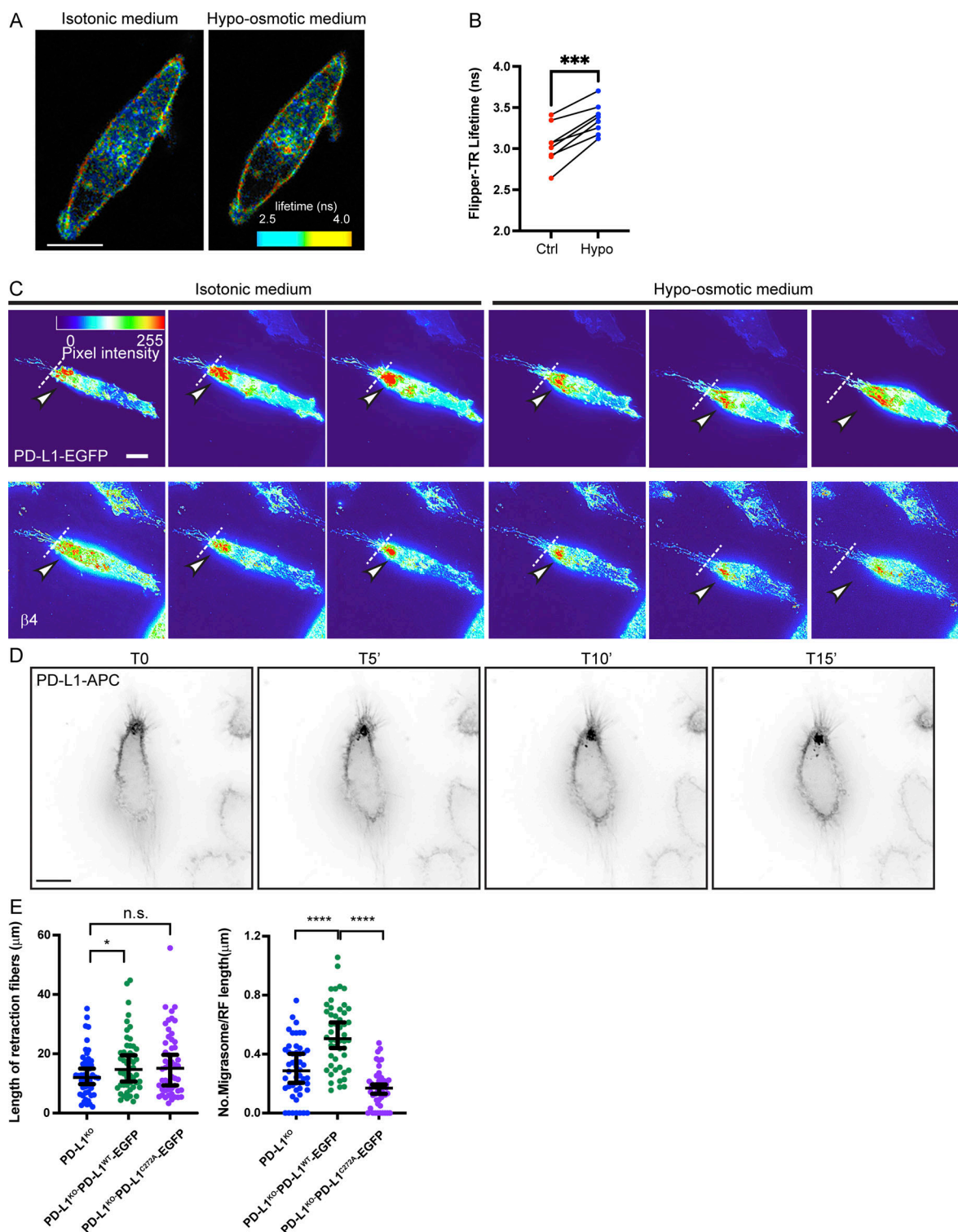
Figure S4. PD-L1 regulates membrane tension to localize β4 to the cell rear. Related to Fig. 4. **(A)** Heat-map images show Flipper-TR lifetime of WT MDA-MB-231 cells in isotonic (left) or hypo-osmotic medium (right). Scale bar: 10 μm. **(B)** Quantification of Flipper-TR lifetime in the same cell in isotonic or hypo-osmotic medium for 5 min. Statistical significance was determined by two-sided paired t test (n = 8 cells). ***, 0.001 > P ≥ 0.0001. **(C)** Pixel intensity map of time-lapse images of PD-L1^{KO}-PD-L1-EGFP MDA-MB-231 cells in isotonic (left) or hypo-osmotic (right) medium shown in Fig. 6 E. Top: Pixel intensity map from PD-L1 single channel only. Bottom: Pixel intensity map from integrin β4 single channel only. White dotted lines indicate rear of the cell. White arrowheads indicate location of PD-L1 (middle) or integrin β4 (bottom). Scale bar: 10 μm. **(D)** Time-lapse microscopy images of PC3 cells pre-labeled with an anti–PD-L1-APC antibody to show PD-L1-APC uptake during persistent cell migration. Scale bar: 10 μm. **(E)** Quantification of retraction fiber length and migrasome numbers/retraction fiber length in PD-L1^{KO}, PD-L1^{KO}-PD-L1-EGFP, and PD-L1^{KO}-PD-L1^{C272A}-EGFP MDA-MB-231. Data are shown as means ± SD from three independent experiments, n > 50 cells per condition. Statistical significance was determined by two-sided unpaired t test. *, 0.05 > P ≥ 0.01; ****, 0.0001 > P.

Video 1. **PD-L1 localizes at retraction fibers and migrasomes in MDA-MB-231 cells.** The movie was taken by imaging PD-L1-EGFP using time-lapse epifluorescence microscopy with 5-min intervals after MDA-MB-231 cells were seeded on the coverslip overnight at 37°C. The images are displayed at 5 frames per second. Notice that PD-L1 first appears highly concentrated at the upper-left edge of the cell and moves toward the cell body as the edge contracts, leaving behind PD-L1 containing retraction fibers and migrasomes. Related images are shown in Fig. 2 A. Scale bar: 10 µm.

Video 2. **PD-L1 localizes at retraction fibers and migrasomes in 4T1 cells.** The movie was taken by imaging PD-L1-EGFP using time-lapse epifluorescence microscopy with 5-min intervals after 4T1 cells were seeded on the coverslip overnight. The images are displayed at 3 frames per second. Notice that PD-L1 first appears highly concentrated at the edge of the cells and moves toward the cell body as the edge contracts, leaving behind PD-L1–containing retraction fibers and migrasomes. Related images are shown in Fig. 2 B. Scale bar: 10 µm.

Video 3. **PD-L1 WT MDA-MB-231 cells form retraction fibers during cell migration.** The movie was taken by imaging SiR-Actin using time-lapse epifluorescence microscopy with 5-min intervals after MDA-MB-231 were seeded on the coverslip overnight and stained with Sir-Actin before imaging. The images are displayed at 2 frames per second. Notice that the PD-L1 WT cell shows clear front–rear polarity and formed retraction fibers at the rear of the cell. Related images are shown in Fig. 2 F. Scale bar: 10 µm.

Video 4. **PD-L1 deletion inhibits retraction fiber formation during cell migration.** The movie was taken by imaging SiR-Actin using time-lapse epifluorescence microscopy with 5-min intervals after PD-L1KO MDA-MB-231 were seeded on the coverslip overnight and stained with SiR-Actin before imaging. The images are displayed at 2 frames per second. Notice that the PD-L1KO cell does not establish front–rear polarity and does not form clear retraction fibers. Related images are shown in Fig. 2 F. Scale bar: 10 µm.

Video 5. **PD-L1 and the β4 integrin co-localize at "roots" of retraction fibers during cell migration.** The movie was taken by imaging PD-L1 (green) and the β4 integrin (red) using time-lapse epifluorescence microscopy with 5-min intervals after 4T1-β4-tdTomato-PD-L1-EGFP cells were seeded on the coverslip overnight. The images are displayed at 1 frame per second. Related images are shown in Fig. 3 G. Scale bar: 10 µm.

Video 6. **Control 4T1 cells form PD-L1 containing retraction fibers.** The movie was taken by imaging PD-L1-EGFP using time-lapse epifluorescence microscopy with 5-min intervals after 4T1-dox-shβ4 cells were seeded on the coverslip for 3 days without dox treatment. The images are displayed at 3 frames per second. Notice that the cell showed clear front–rear polarity and formed retraction fibers at the rear of the cell. Related images are shown in Fig. 4 D. Scale bar: 10 µm.

Video 7. **Knock-down of the β4 integrin inhibits retraction fiber formation in 4T1 cells.** The movie was taken by imaging PD-L1-EGFP using time-lapse epifluorescence microscopy with 5-min intervals after 4T1-dox-shβ4 cells were seeded on the coverslip and treated with dox for 3 days. The images are displayed at 3 frames per second. Notice that the cells did not establish front–rear polarity and did not show persistent cell migration. Related images are shown in Fig. 4 D. Scale bar: 10 µm.